IMU-INTEGRATED ‘SMART’ KNEE BRACE VALIDATION USING OPTOELECTRONIC MOTION CAPTURE DURING TREADMILL WALKING

VINCENT NGUYEN

A THESIS SUBMITTED TO THE FACULTY OF GRADUATE STUDIES IN PARTIAL FULFILLMENT OF THE REQUIREMENTS FOR THE DEGREE OF MASTER OF SCIENCE

GRADUATE PROGRAM IN KINESIOLOGY AND HEALTH SCIENCE

YORK UNIVERSITY

TORONTO, ONTARIO

August 2024

ABSTRACT

Optoelectronic motion capture systems are the gold standard for collecting kinematic data. However, these systems are expensive, occupy a large volume of space, and require training to operate. Inertial measurement units (IMUs) are small, portable devices that measure linear acceleration, angular velocity, and magnetic field and have been proven to be valid in measuring joint angles. A ‘smart’ brace was implemented with two IMUs and the knee joint angles calculated using data from the ’smart’ brace were compared to a gold standard motion capture system to assess the agreement and reliability of the brace. Ten participants visited the lab for two sessions, during which three 2-minute treadmill walking trials were conducted each session. The ‘smart’ brace had moderate to excellent reliability in measuring axial plane range of motion, and sagittal and frontal plane knee angles, but had poor agreement when measuring sagittal plane angles and frontal plane range of motion.

ACKNOWLEDGMENTS

This thesis is dedicated to every individual who has played a role in its completion during my time in graduate school. I would like to start by acknowledging my defense committee members: Dr. William Gage, Dr. Garrett Melenka, and Dr. George Mochizuki. Thank you for all your contributions in helping me complete this thesis. Will, I am immensely grateful to you for being my supervisor throughout my master’s degree and am truly grateful for the knowledge, guidance, and wisdom that you have provided me. The mentorship you have provided me in my academic, personal, and professional life is deeply appreciated. You have not only helped me become a better researcher, but also enabled me to think critically when navigating the world.

Next, I’d like to thank Rahim Dhupalia, Dr. Garrett Melenka, and Dr. Gerd Grau from the Lassonde School of Engineering for creating the ‘smart’ brace and making my interdisciplinary thesis possible. I could not have done it without your engineering knowledge and expertise. Rahim, you taught me how to code and I am truly grateful for the camaraderie we shared throughout graduate school.

Finally, I’d like to thank my family, friends, current, past, and present lab mates for all their love and support. I’d especially like to thank Dr. Vincenzo Di Bacco and Cecilia Power for your guidance in navigating through my master’s degree. I could always count on you guys for help, whether it was troubleshooting equipment in the lab, learning statistics, or simply providing advice on how to get through grad school. Last, but not least, I’d like to thank Traian Bursu for your companionship throughout graduate school. Our friendship started on day one of the master’s program and you have pushed me to persevere until the very end.

TABLE OF CONTENTS

LIST OF TABLES

LIST OF FIGURES

LIST OF EQUATIONS

LIST OF ACRONYMS AND ABBREVIATIONS

IMU	Inertial Measurement Unit
IRED	Infrared Light Emitting Diode
RMSE	Root Mean Square Error
AHRS	Attitude and Heading Reference System
PWS	Preferred Walking Speed
LCS	Local Coordinate System
LOA	Limits of Agreement
ICC	Intraclass Correlation
ANOVA	Analysis of Variance

1.0 INTRODUCTION

Walking, or the ability to perform gait is a key component of daily functional living for the majority of people. The analysis of human gait allows researchers and clinicians to examine, analyze, and monitor the prevalence of diseases and injuries affecting the lower body. Optoelectronic motion capture has been used for several years in biomechanics laboratories to measure kinematic parameters during gait. Although these motion capture systems are regarded as the gold standard for collecting kinematic data, they are extremely expensive to obtain, require a large volume of space, and high level of expertise to operate. Emerging technology using inertial measurement units (IMUs) to measure linear acceleration, angular velocity, and magnetic field have been proven to accurately and precisely record knee joint angle during gait (Al-Amri et al., 2018; Binnie et al., 2021; Cooper et al., 2009; Kayaalp et al., 2019; Park & Yoon, 2021). We now live in a digital era, where technology surrounds us and has become an integral part of our daily lives, shaping how we communicate, work, and interact with the environment and people around us. ‘Smart’ healthcare technology is a term that can be used to identify wearable technology that is used to monitor and track biophysical data (Tian et al., 2019). For example, smartphones or watches that record the wearer’s daily step count, heart rate, blood pressure, sleep cycle, and more. IMUs can be integrated into devices, such as knee braces, to create ‘smart’ braces that collect biophysical data over an extended period, during normal activities of daily living. The data collected from ‘smart’ braces could allow clinicians and medical professionals to monitor patient function outside the laboratory or clinic. The aim of this thesis is therefore to validate an IMU-instrumented ‘smart’ knee brace against a gold standard motion capture system in measuring the knee joint angles in all three planes of motion.

2.0 LITERATURE REVIEW

2.1 KNEE JOINT AND GAIT KINEMATICS

The knee is a hinge joint with motion primarily in the sagittal plane. Although the principal movement is flexion and extension, there are also smaller rotations in the varus/valgus direction (i.e., frontal plane), and internal/external (i.e., axial plane) rotation (Abulhasan & Grey, 2017). The muscles involved in knee flexion are the biceps femoris, semimembranosus, semitendinosus, gastrocnemius, plantaris, gracilis, and popliteus (Gupton, Imonugo, & Terreberry, 2022). Knee extension is achieved by activating the rectus femoris, vastus medialis, vastus lateralis, and vastus intermedius, which collectively make up the quadriceps femoris (Gupton et al., 2022). The coordination of knee flexors and extensors therefore establishes the fundamental role of the knee during gait.

The gait cycle is often defined from the start of heel contact of the foot to the next heel contact of the same foot (Robertson, Caldwell, Hamill, Kamen, & Whittlesey, 2014). For each foot, there are two main phases in the gait cycle, the stance phase and the swing phase. The stance phase spans 60% of the gait cycle and occurs while the foot is in contact with the ground (Abid, Mezghani, & Mitiche, 2019). The swing phase on the other hand, encompasses the remaining 40% and is when the foot is not in contact with the ground (Abid et al., 2019). There are four notable events when looking at the waveform of sagittal knee joint angle for a healthy individual during gait, as shown in Figure 1. Point 1 on Figure 1 is the first period of flexion and occurs immediately after the initial heel contact, at the beginning of the loading phase, as the weight of the body is being loaded onto the limb (Abid et al., 2019; Ahn & Hogan, 2012; Gage, 1990). Next, a period of knee extension, point 2 on Figure 1, occurs during the terminal stance phase as the heel begins to lift from the ground. As the leg proceeds through the swing phase, the point of maximum knee flexion, point 3 on Figure 1, occurs to ensure that the foot is raised high enough to be clear of the ground. The leg then goes through the largest bout of knee extension, point 4 on Figure 1, at the end of the gait cycle, adjacent to heel contact.

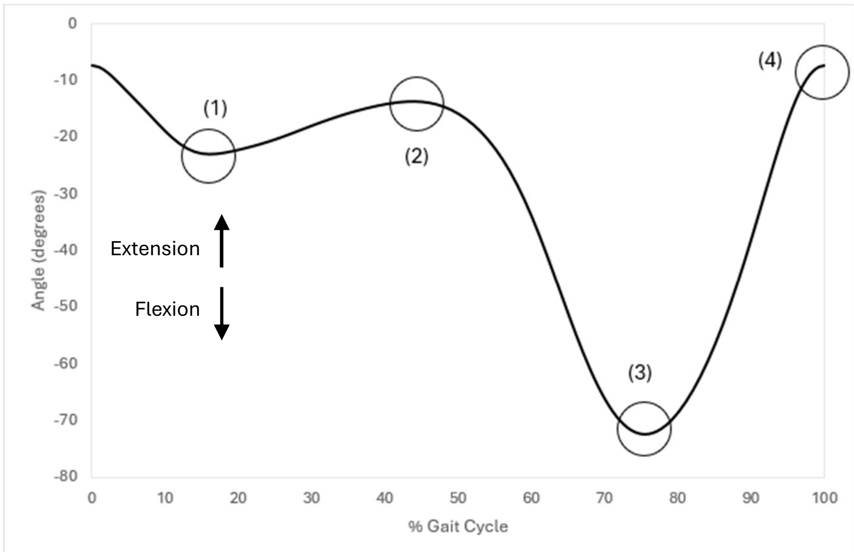

Figure 1. Waveform of sagittal knee joint angle during a gait cycle for healthy individuals. A negative angle indicates that the knee is in a flexed position and a positive angle indicates that the knee is in an extended position. The four main events in the waveform are (1) maximum knee flexion during the initial loading phase, (2) maximum knee extension during terminal stance phase, (3) maximum knee flexion during swing phase, and (4) maximum knee extension adjacent to heel contact (Abid et al., 2019; Ahn & Hogan, 2012; Gage, 1990).

The knee joint has an important role in the stability of the lower limbs for a healthy gait pattern. The joint ensures that the femur and tibia are held stable when bearing weight and concurrently mobile enough to flex or extend when required. During the terminal 20 degrees of full extension, the tibia is externally rotated by about 15 degrees in a process called the ‘screw-home mechanism’ (Kim et al., 2015). The knee is put in a ‘locked’ position where the femur and tibia are stabilized. The popliteus initiates knee flexion by ‘unlocking’ the knee when it is ‘locked’. When the tibia and femur are in a weight-bearing state, such as the stance phase of gait, the popliteus will externally rotate the femur on the tibia (Jadhav, More, Riascos, Lemos, & Swischuk, 2014). When in a non-weight-bearing state, such as the swing phase of gait, the popliteus will internally rotate the tibia on the femur to ‘unlock’ the knee (Jadhav et al., 2014). To summarize, the knee joint has a crucial role in providing functional movement and the stabilization of the lower limbs during gait.

2.2 OPTOELECTRONIC MOTION CAPTURE

Optoelectronic motion capture systems are commonly used in biomechanics research to record and analyze human kinematics. These systems require the simultaneous operation of multiple infrared cameras to view markers, which are placed on strategic anatomical locations on the participant, in two dimensions and, using software, reconstruct them in three-dimensional space. The markers are used to create body segments and kinematics are calculated, also using motion capture software. Optoelectronic motion capture systems can operate actively or passively (De Guise, Mezghani, Aissaoui, & Hagemeister, 2011). Passive systems utilize cameras that simultaneously emit and detect infrared light reflected off spherical markers covered in infrared reflective tape (De Guise et al., 2011; Robertson et al., 2014). Passive systems require at least two cameras to reconstruct a single marker in three-dimensional space (Robertson et al., 2014). However, a multicamera system where each marker is always in view of at least two cameras is beneficial if markers become obstructed while the subject is in motion (Robertson et al., 2014). Where passive systems utilize freestanding markers, active motion capture systems use infrared light emitting diodes (IREDs) that are cabled and require a power source (De Guise et al., 2011; Robertson et al., 2014; Winter, 2009). Once attached to a participant, IREDs emit infrared light in a pulsing sequence that is detected by a series of cameras for marker identification (De Guise et al., 2011; Robertson et al., 2014; Winter, 2009). Both active and passive motion capture systems are widely used and useful tools in biomechanical research.

2.3 INERTIAL MEASUREMENT UNITS

Inertial measurement units are small, portable devices that contain accelerometers, gyroscopes, and magnetometers to sense linear acceleration, angular velocity, and magnetic field, respectively. Since a singular sensor can only measure changes in one axis, a trio of each sensor are aligned in an orthogonal manner to assess fluctuations of linear acceleration, angular velocity, or magnetic field in three dimensions (Iosa, Picerno, Paolucci, & Morone, 2016). To accurately assess human motion, IMUs need to be rigidly affixed to body segments to avoid motion artifacts (Iosa et al., 2016). Previous studies have attached IMUs to the leg and thigh to measure knee joint kinematics (Al-Amri et al., 2018; Binnie et al., 2021; Dejnabadi, Jolles, & Aminian, 2005; Kayaalp et al., 2019; Park & Yoon, 2021; Robert-Lachaine, Mecheri, Larue, & Plamondon, 2016; Seel, Raisch, & Schauer, 2014). When testing the validity of IMUs against a gold standard motion capture system, Kayaalp et al. (2019) found that the two systems did not have any significant differences in measuring maximum knee flexion angles or sagittal range of motion but differed in measuring the extension angle during stance phase. Cooper et al. (2009) found that IMUs displayed excellent agreement with the motion capture system in estimating knee joint angle, having a root mean square error (RMSE) of 0.7 and 3.4 degrees during walking speeds of one and five miles per hour, respectively, indicating that accuracy decreased as gait speed increased. The correlation between the sagittal knee angle of a reference ultrasound-based motion measurement system and accelerometer and gyroscope integrated sensor was found to have a correlation coefficient of 0.997 during treadmill walking (Dejnabadi et al., 2005). The literature makes it clear that IMUs have been used successfully in estimating knee joint angles when secured to the thigh and lower leg, however, evidence for the validation of a ‘smart’ knee brace instrumented with IMUs is still lacking.

2.4 IMU SENSOR FUSION

Modern electronics contain a wide variety of sensors that are used to detect and measure fluctuations occurring in the surrounding environment. Sensor fusion is the process by which signals from multiple sensors are integrated to produce a more accurate and reliable signal or measurement (Sasiadek, 2002). When relying solely on the three accelerometers within an IMU, the roll and pitch angles can be calculated by detecting gravitational acceleration while the IMU is in a static state. However, measurements become highly inaccurate when the IMU is in a dynamic state and larger, external accelerations are detected (NXP, 2015). Although the gyroscopes can be used to measure the orientation of an IMU by integrating the change in orientation for all three axes, the signal of the orientation angle will drift for longer-duration recordings (Nazarahari & Rouhani, 2021). It should be noted that signal drift would also be prevalent if accelerometer data were integrated to determine velocity or displacement for longer durations. Magnetometers can be used to determine the direction of magnetic north, but the signal is inaccurate when ferrous materials are brought near the IMU and can be disrupted by electronics within the IMU that disturb the magnetic field (Nazarahari & Rouhani, 2021). An attitude and heading reference system (AHRS) filter is a type of sensor fusion algorithm that can combine data collected from accelerometers, gyroscopes, and magnetometers to accurately calculate the roll, pitch, and yaw orientation of an IMU (Nazarahari & Rouhani, 2021). The global coordinate system used is typically a North-East-Down reference frame where east is determined from the cross-product of the north and down vectors, which are the geomagnetic north and gravity vectors, respectively, and the IMU is a local coordinate system rotating in the global coordinate system (“Determine Orientation Using Inertial Sensors,” n.d). When the three types of sensors in the IMU are integrated, the magnetometers counteract the drift that is present when integrating gyroscope data and the gyroscopes can stabilize magnetic north for yaw (NXP, 2015). The accelerometers are used to calculate the pitch and roll angles, but when external accelerations are present, the gyroscopes can identify whether the IMU is actually rotating (Widodo & Wada, 2016). To conclude, sensor fusion algorithms are useful tools that can integrate data from multiple sensors to produce a reliable estimation of an IMU's three-dimensional orientation.

3.0 RESEARCH QUESTION AND HYPOTHESIS

This study was designed to test the validity and reliability of an instrumented 'smart' knee brace against a gold standard motion capture system. To be specific, the knee joint angles derived using signals detected by the IMUs on the 'smart' brace and knee joint angles derived using an optoelectronic camera-based motion capture system were compared during bouts of treadmill walking. This approach was used to test the accuracy and precision of the 'smart' brace in measuring the knee kinematics of young, healthy participants during gait. The validation of the 'smart' brace was of particular importance because it would provide a more cost-effective and convenient method for researchers to analyze knee kinematics. Regarding previous literature on IMUs and knee kinematics, this thesis has posed the following research questions:

(1) Will the IMU integrated 'smart' knee brace be able to measure knee joint angles to the same degree of accuracy and precision as the gold standard optoelectronic motion capture system during treadmill walking?

It was hypothesized that the 'smart' knee brace would demonstrate good reliability and agreement with the gold standard optoelectronic motion capture system when measuring knee joint angles during treadmill walking.

The remainder of this thesis document presents two phases in which the ‘smart’ brace was validated against the gold standard motion capture system. Phase 1 validated the output of the accelerometers and gyroscopes of the IMUs on the ‘smart’ brace against the motion capture system. Phase 2 incorporated the use of sensor fusion algorithms which integrated the accelerometers, gyroscopes, and magnetometers in the IMUs to calculate their orientation and then relative knee angle in all three planes of motion. Phase 1 and 2 will each have a methods and results section to explain the evolution of the process in which the ‘smart’ brace was validated against the gold standard motion capture system.

4.0 PHASE 1

4.1 METHODS

4.1.1 OVERVIEW OF PROTOCOL

Approval to conduct the experiments that engaged human participants contained in this thesis was obtained through York University’s Office of Research Ethics: Certificate #STU 2023-024, *‘Smart’ Knee Brace Validation Study*. A pilot study was conducted to evaluate the validity of the accelerometers and gyroscopes within two SparkFun ICM-20948 IMUs (SparkFun, Niwot, CO, USA), which were integrated into a compression knee sleeve to create a ‘smart’ brace. One young, healthy female participant (age = 21 years, mass = 48.6 kg, height = 1.63 meters) without any history of neurological or musculoskeletal disorders volunteered to participate in this pilot study. The participant completed a preferred walking speed test (PWS) at the beginning of the session to determine their natural gait speed (Kiriella, Di Bacco, Hollands, & Gage, 2020, Marmelat, Torre, Beek, & Daffertshofer, 2014). In the first half of the PWS test, the participant walked on the treadmill at a belt speed they verbally indicated was too slow compared to their natural walking speed. The belt speed was then increased by increments of 0.10 miles/hour every 10 seconds until the participant verbally indicated they were walking at their natural walking speed. The belt speed was then increased to a speed the participant verbally indicated was too fast compared to their natural walking speed. The treadmill belt speed was then decreased by increments of 0.10 miles/hour every 10 seconds until the participant verbally indicated they were at their natural walking speed. The two speeds that the participant indicated were their natural walking speeds from the first and second half of the PWS test were averaged, and this speed was used for the remainder of their treadmill walking trials. The participant was blinded to the current belt speed value until after their preferred walking speed was calculated. After the PWS was completed, the participant was asked to jog at a comfortable pace, which was a belt speed they felt comfortable jogging for 10 minutes. The speed they selected would then be used as their jogging speed for the remainder of the treadmill jogging trials. After the preferred walking and jogging speeds were selected, the participant wore the 'smart' knee brace on their right knee and infrared reflective markers were placed on strategic anatomic locations on their lower body, as shown in Figure 2 and Table 1. The participant wore a harness that was affixed to the ceiling for the treadmill walking and jogging trials to prevent any injuries from occurring if they were to fall. After the equipment was set up, the participant performed three trials of 2 minute treadmill walking at their PWS, three trials of 10 squats to parallel during which the descent and ascent were approximately 1 second each, three trials of 10 sit-to-stand movements during which the participant paused for approximately 1 second after sitting and 1 second after standing, three trials of 10 alternating lunges during which the participant paused for approximately 1 second after each lunge, and three trials of 2 minute treadmill jogging at a self-selected pace. At the beginning of every trial, the participant stood still for 10 seconds, performed two knee flexions with the right leg, then stood still for 5 seconds, before the required movement was conducted. The participant was able to rest for as long as needed after every trial. Only the treadmill walking data were retained for the purposes of this study; the other data were collected for the purposes of an associated project focused on machine learning to categorize movements.

4.1.2 EQUIPMENT AND MEASURES

A motorized treadmill (Bodyguard Fitness, Quebec, Canada) was used to enable data collection over an extended period of uninterrupted walking. Seven MX series optoelectronic motion capture cameras (MX40, Vicon, Denver, CO, USA) were strategically positioned around the lab space to collect participants' movement, which sampled at 100 Hz. Twenty-eight reflective markers were placed in strategic anatomic locations on the lower body (C-Motion Wiki Documentation, 2017) using double-sided adhesive tape, as shown in Figure 2 and Table 1. A compression knee brace with a SparkFun ICM-20948 IMU positioned at both ends of the brace, as shown in Figure 3, was used to collect linear acceleration, angular velocity, and magnetic field signals in the triaxial planes of movement; IMU signals were sampled at 80 Hz. The SparkFun IMUs were positioned at mid-thigh and mid-shank, respectively, when the 'smart' brace was worn on the right leg. A triangular plate with three reflective markers, attached and arranged noncollinearly, was placed directly on top of each SparkFun IMU. The plates were attached to the IMUs using Velcro and secured using a strap that wrapped around the thigh or shank. The two IMUs on the 'smart' brace collected data points asynchronously, with the IMU at the thigh collecting a data point first, then IMU at the shank collecting a data point 6 or 7 milliseconds after and repeating the process over again. Data from the SparkFun IMUs were saved on an SD card in a housing unit, which was worn around the participant's waist.

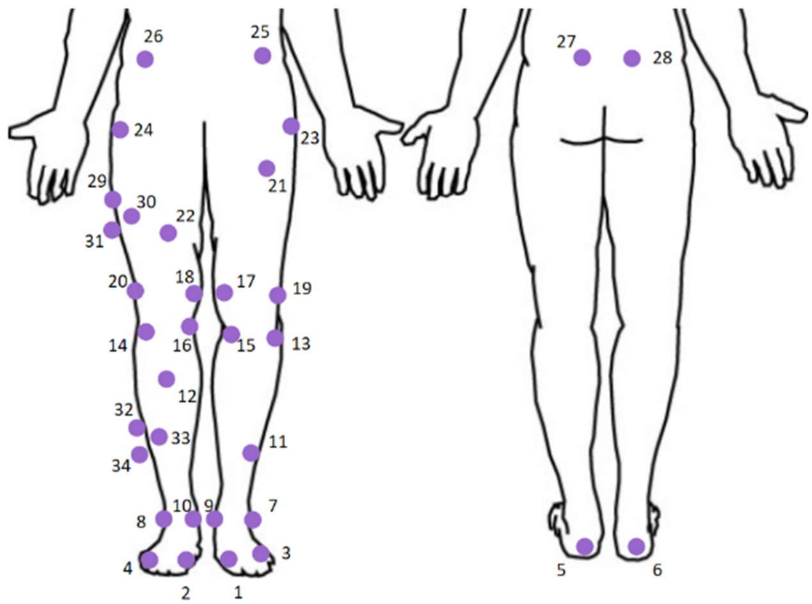

Figure 2: Marker placement of the thirty-four reflective markers used for 3D motion capture.

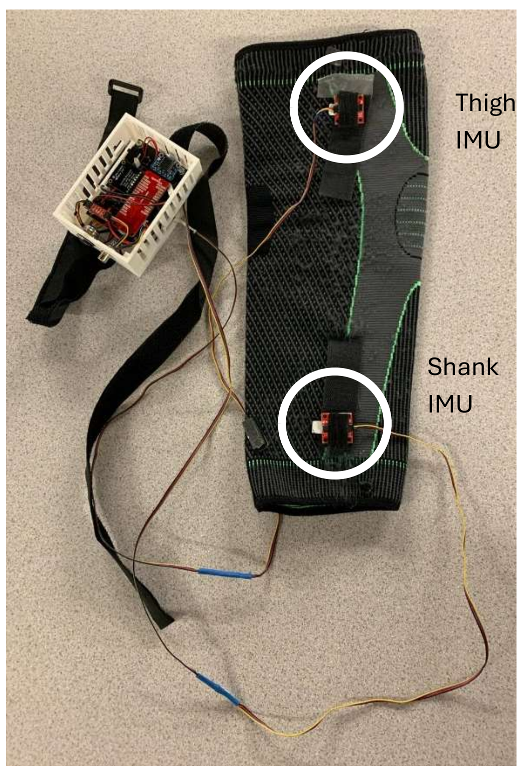

Figure 3: The 'smart' brace with thigh and shank IMU connected to the data recording box.

Table 1: Marker name and corresponding anatomic location of each marker required for motion capture. Marker placements were based on the C-Motion Wiki Documentation under the 'Marker Set Guidelines' page.

	Marker Name	Marker Anatomic Location		Marker Name	Marker Anatomic Location
1	LFM1	Left distal aspect of 1st metatarsal	2	RFM1	Right distal aspect of 1st metatarsal
3	LFM5	Left distal aspect of 5th metatarsal	4	RFM5	Right distal aspect of 5th metatarsal
5	LCA	Left posterior calcaneus	6	RCA	Right posterior calcaneus
7	LFAM	Left fibula, apex of lateral malleolus	8	RFAM	Right fibula, apex of lateral malleolus
9	LTAM	Left tibia, apex of medial malleolus	10	RTAM	Right tibia, apex of medial malleolus
11	LSK	Anterior crest of left tibia	12	RSK	Anterior crest of right tibia
13	LLTC	Left lateral tibial condyle	14	RLTC	Right lateral tibial condyle
15	LMTC	Left medial tibial condyle	16	RMTC	Right medial tibial condyle
17	LFME	Medial condyle of left femur	18	RFME	Medial condyle of right femur
19	LFLE	Lateral condyle of left femur	20	RFLE	Lateral condyle of right femur
21	LTH	Anterior surface of left thigh	22	RTH	Anterior surface of right thigh
23	LFT	Greater trochanter of left femur	24	RFT	Greater trochanter of right femur
25	LIAS	Left anterior superior iliac spine	26	RIAS	Right anterior superior iliac spine
27	LIPS	Left posterior superior iliac spine	28	RIPS	Right posterior superior iliac spine
29	TT IMU	Top Thigh IMU			
30	FT IMU	Front Thigh IMU			
31	BT IMU	Bottom Thigh IMU			
32	TS IMU	Top Shank IMU			
33	FS IMU	Front Shank IMU			
34	BS IMU	Bottom Shank IMU			

4.1.3 DATA PROCESSING

Motion capture and IMU data were processed through a series of four different experiments to test the validity of the accelerometers and gyroscopes in the IMUs during treadmill walking. The first experiment, called Linear Accelerations of Plate Centroid, involved averaging the positions of the three noncollinear markers on the plates attached to the thigh and shank IMUs to create a centroid on each of the thigh and shank plates. The triaxial accelerations of each of the centroids were then compared to the triaxial linear accelerations measured by the thigh and shank IMUs, respectively. This experiment was performed to compare the linear acceleration measured in each of the X, Y, or Z axes between both systems. The second experiment, called Vector Sum of Accelerations, involved calculating and comparing the vector sum of the acceleration in all three axes for the top thigh IMU marker and the bottom shank IMU marker to the vector sum of the acceleration in all three axes for the IMUs at the thigh and shank, respectively. This experiment was performed to compare the resultant acceleration vector between the two systems since the coordinate axes between the motion capture system and IMUs were not perfectly aligned. The third experiment, called Angular Velocities of Plate, involved creating a local coordinate system (LCS) for each of the plates on the thigh and shank IMUs. The triaxial angular velocities of each of the LCSs were then compared to the triaxial angular velocities measured by each of the thigh and shank IMUs, respectively, to validate the gyroscopes on the IMUs. Finally, the fourth experiment, called Gravitational Acceleration Angle, involved calculating sagittal knee joint angles using gravitational acceleration measured by the thigh and shank IMUs and comparing it to the sagittal knee angles recorded by the motion capture system. This experiment was performed to examine if sagittal knee joint angle could be estimated using the acceleration of gravity sensed by the accelerometers in the IMUs. Motion capture data were filtered in Visual3D using a 4^{th} order low-pass Butterworth filter with a cut-off frequency of 6Hz (Winter, 2009) for all four experiments. The X axis was oriented positive to the right, Y axis was positive anteriorly, and Z axis was positive up vertically, in the motion capture space. For the IMUs, the X axis was oriented positive to the right (laterally), Y axis was positive anteriorly, and Z axis was aligned with the longitudinal axis of the thigh or shank, positive upward.

4.1.3.1 LINEAR ACCELERATIONS OF PLATE CENTROID DATA PROCESSING

The IMU data were filtered in MATLAB R2023a (The Mathworks, Natick, MA, USA) using a 4th order low-pass Butterworth filter with cut-off frequencies based on a residual analysis (Winter, 2009), before being interpolated to 100 Hz, using the interp1() function in MATLAB, to match the motion capture sampling rate. The acceleration data for the thigh and shank IMUs in the X, Y, and Z axes were filtered with cut-off frequencies of 4 Hz, 4 Hz, 4 Hz, 5 Hz, 4 Hz, and 5 Hz, respectively. The positions of the three noncollinear markers on the plates attached to each of the thigh and shank IMUs were averaged to calculate a centroid for each of the plates. The position of each centroid was double-differentiated, using the finite difference method (Winter, 2009), to calculate and compare the triaxial accelerations of the centroids to the triaxial linear accelerations measured by the IMUs. Gravitational acceleration, which had a constant of -9.81 m/s^2 in the Z axis of the thigh and shank IMUs, was removed from the acceleration signals of both IMUs by adding 9.81 m/s^2 to every datapoint in the Z axis.

4.1.3.2 VECTOR SUM OF ACCELERATIONS DATA PROCESSING

The IMU data were filtered and interpolated as was done in the data processing method for Linear Accelerations of Plate Centroid. The vector sum of the acceleration signals in the X, Y, and Z axes was then calculated at each timepoint, for both the thigh and shank IMUs. The filtered position data of the top thigh IMU and bottom shank IMU markers were double-differentiated using the finite difference method to produce acceleration signals in the X, Y, and

Z axes (Winter, 2009). The value of acceleration due to gravity, $9.81 m/s^2$, was as subtracted from every datapoint in the Z axis acceleration signal, which was the vertical axis in the motion capture space, to account for gravitational acceleration, and the vector sum of the acceleration signals for the X axis, Y axis, and Z axis with gravitational acceleration was calculated for both the top thigh IMU and bottom shank IMU markers.

4.1.3.3 ANGULAR VELOCITIES OF PLATE DATA PROCESSING

The IMU data were filtered in MATLAB using a 4^{th} order low-pass Butterworth filter with cut-off frequencies based on a residual analysis (Winter, 2009), before being interpolated to 100 Hz, using the interp1() function in MATLAB, to match the motion capture sampling rate. The angular velocity data for the thigh and shank IMUs in the X, Y, and Z axes were filtered with cut-off frequencies of 4 Hz, 5 Hz, 4 Hz, 4 Hz, 4 Hz, and 4 Hz, respectively. An LCS was created for each of the plates that were placed on the thigh and shank IMUs using the three noncollinear markers that were attached to each of the plates. The LCSs were oriented such that the x axis was positive to the right, y axis was positive anteriorly, and z axis was positive up vertically, with $\widehat{\iota'}$, $\widehat{\jmath'}$, and $\widehat{k'}$ representing the unit vectors for each of the axes, respectively. Equation (1) was used to calculate the angular displacement around each of the x, y, and z axes using the x, y, or z components for each of the $\widehat{\iota'}$, $\widehat{\jmath'}$, and $\widehat{k'}$ unit vectors:

$$\theta = tan^{-1}(\frac{o}{a}) \tag{1}$$

Where o is the $\hat{\imath}'_z$ component and a is the $\hat{\imath}'_x$ component of the $\widehat{\iota'}$ unit vector when calculating rotation around the y axis. When calculating the rotation around the z axis, o is the $\hat{\jmath}'_x$ component and a is the $\hat{\jmath}'_y$ component of the $\widehat{\jmath'}$ unit vector. When calculating the rotation around the x axis, o is the $\hat{k}'_y$ component and a is the $\hat{k}'_z$ component of the $\widehat{k'}$ unit vector. θ is subtracted by 180 when both $\hat{k}'_y$ and $\hat{k}'_z$ are negative, but 180 is added to θ when $\hat{k}'_z$ is negative and $\hat{k}'_y$ is positive to enable displacement angles around the x axis in the ranges from -90 to -180 degrees and 90 to 180 degrees, respectively.

The angular displacements around each of the x, y, and z axes of the LCSs were differentiated using the finite difference technique (Winter, 2009) and the triaxial angular velocities of the LCSs were compared to the triaxial angular velocities measured by the IMUs, respectively.

4.1.3.4 GRAVITATIONAL ACCELERATION ANGLE DATA PROCESSING

The acceleration data recorded in all three axes from the IMUs were filtered in MATLAB using a 4^{th} order low-pass Butterworth filter with a cut-off frequency of 1 Hz to isolate the acceleration of gravity, before being interpolated to 100 Hz, using the interp1() function in MATLAB, to match the motion capture sampling rate. The vector sums of the X, Y, and Z acceleration data measured by the IMUs were calculated at each timepoint, for every trial. The absolute angles of the thigh and shank IMUs in the sagittal plane were calculated, as seen in (2), using the acceleration measured by the IMUs in the Z axis, which is consistent with the longitudinal axes of the thigh and shank, and the vector sum of the accelerations of the IMUs in the X, Y, and Z axes:

$$\theta = cos^{-1}(\frac{a}{h}) \qquad (2)$$

Where a is the acceleration of the IMU in the Z axis and h is the vector sum of the accelerations in the X, Y, and Z axes for the same IMU.

The absolute angle of the thigh IMU was then subtracted by the absolute angle of the shank IMU in the sagittal plane to obtain the sagittal knee angle (Winter, 2009).

4.2 RESULTS

4.2.1 LINEAR ACCELERATIONS OF PLATE CENTROID RESULTS

Upon visual inspection of the graphs of linear acceleration in the X, Y, and Z axes in Figure 4, it was seen that the periodicity of the thigh IMU signals was similar to the acceleration signals of the centroid on the plate attached to the thigh, especially in the Y and Z axes. However, the peaks and troughs of the acceleration signal in the X axis and every second trough of the acceleration signal in the Y axis of the thigh IMU were not similar to their respective thigh plate centroid acceleration signals. Similar results were seen for the shank IMU and the centroid on the plate attached to the shank.

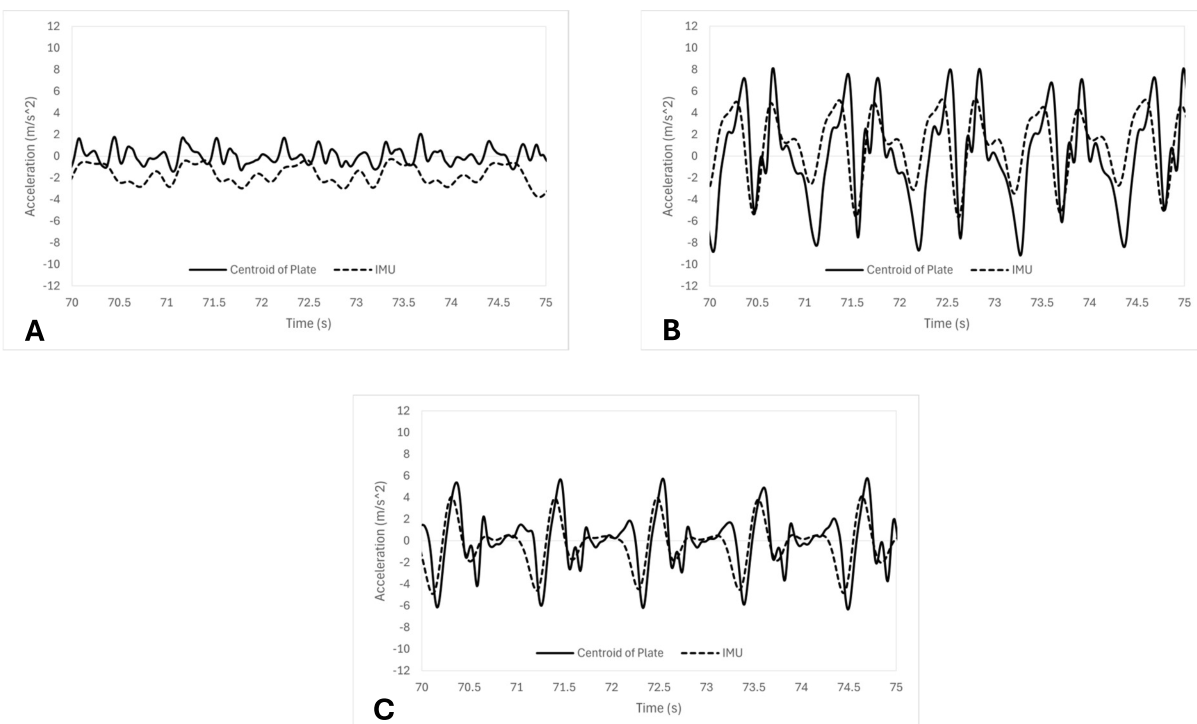

Figure 4. Linear acceleration of the centroid of the three noncollinear markers on the plate on the thigh (solid) and IMU at the thigh (dashed) during a trial of treadmill walking in the (A) X axis, (B) Y axis, and (C) Z axis. Four strides are shown in the figures.

4.2.2 VECTOR SUM OF ACCELERATIONS RESULTS

Upon visual inspection of the graph of acceleration vector sums of the IMU at the thigh and top thigh IMU marker in Figure 5, it was observed that although the IMU was able to match the periodicity and to a certain degree, the amplitude of the motion capture signal, the IMU signal did not reflect the rapid changes in acceleration observed in the motion capture data. Similar results were seen for the IMU at the shank and the bottom shank IMU marker.

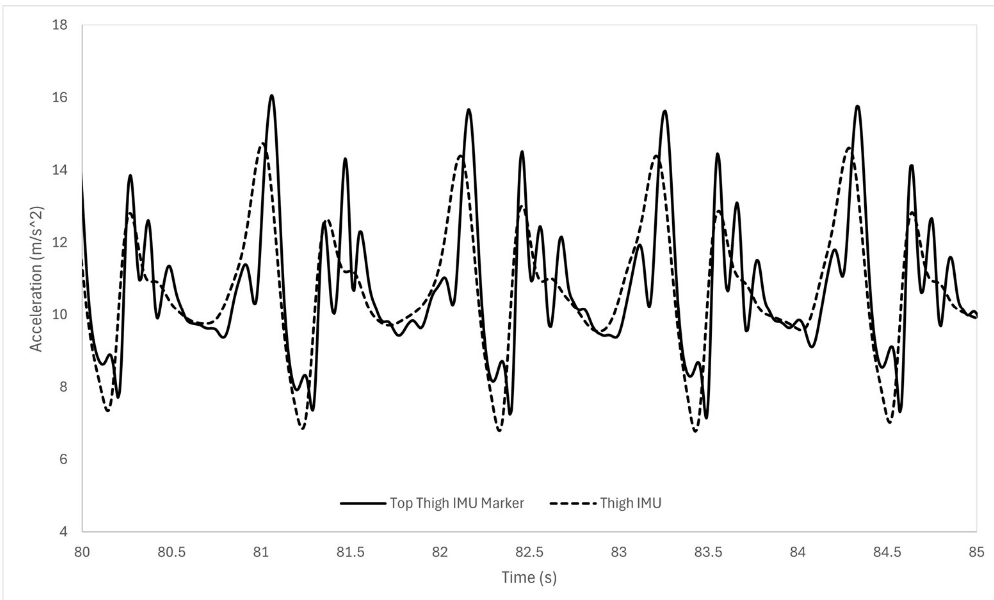

Figure 5. Vector sum of acceleration in the X, Y, and Z axes for the top thigh IMU marker (solid) and IMU accelerations at the thigh (dashed) during a trial of treadmill walking. Four strides of gait are shown in the figure.

4.2.3 ANGULAR VELOCITIES OF PLATE RESULTS

Upon visual inspection of the graphs of angular velocities between the shank IMU and the LCS of the plate on the shank in Figure 6, it was seen that both signals were very similar in the medio-lateral axis. Although the periodicity of the angular velocity signals of the two systems were the same in the antero-posterior and longitudinal axes, the peaks and troughs of the shank IMU signal in the antero-posterior axis were not the same nor as large as those of the LCS of the plate on the shank. Also, the troughs of the angular velocity signal for the shank IMU in the longitudinal axis were too low and not similar to the LCS of the plate attached to the shank IMU. Similar results were seen for the angular velocity signals of the thigh IMU and the LCS of the plate on the thigh.

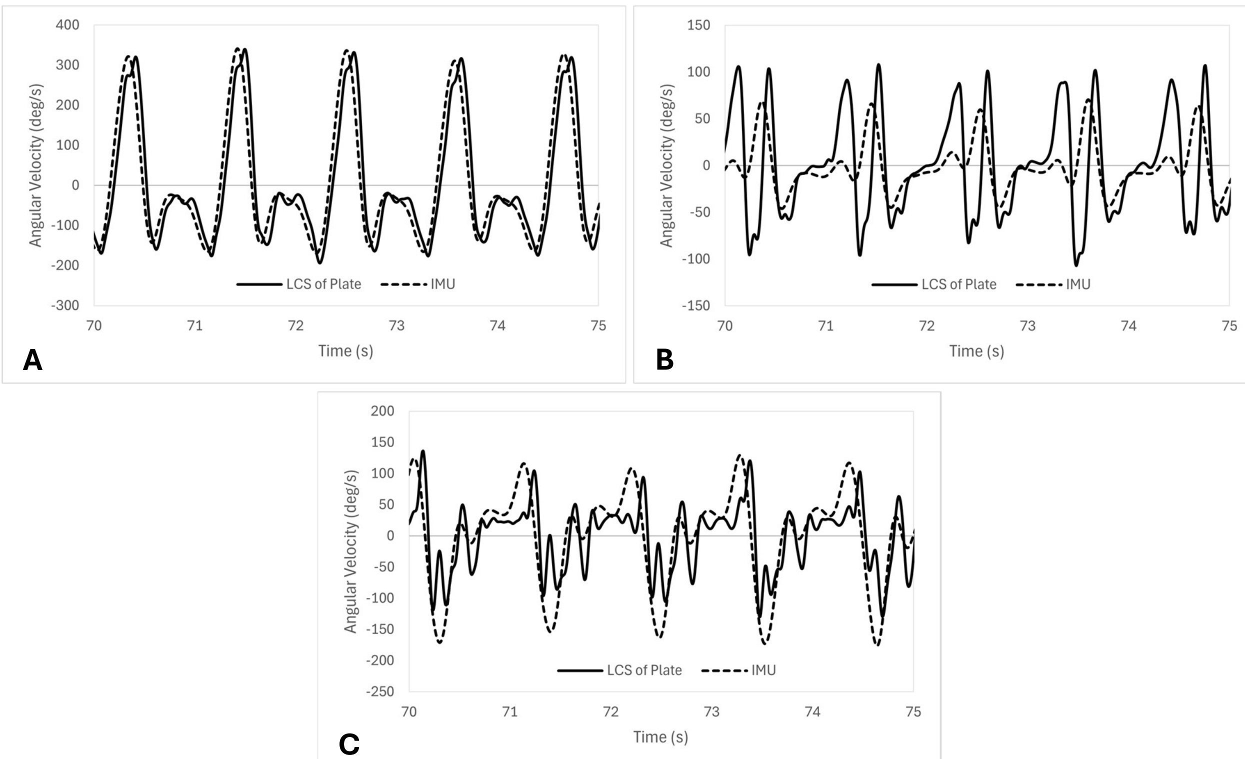

Figure 6. Angular velocity of the LCS for the plate on the shank (solid) and IMU at the shank (dashed) during a trial of treadmill walking around the (A) medio-lateral axis, (B) antero-posterior axis, and (C) longitudinal axis. Four strides are shown in the figures.

4.2.4 GRAVITATIONAL ACCELERATION ANGLE RESULTS

Upon visual inspection of the sagittal knee joint angle signals recorded by the motion capture system and calculated using the acceleration of gravity measured by the IMUs in Figure 7, it was seen that the periodicity of the signals was the same, but the shape of the signals were not similar at all. The signal of sagittal knee angle calculated using gravitational acceleration sensed by the IMUs had a shape similar to a sine wave, where the motion capture signal was bimodal, and the amplitude of the IMU signal was too small.

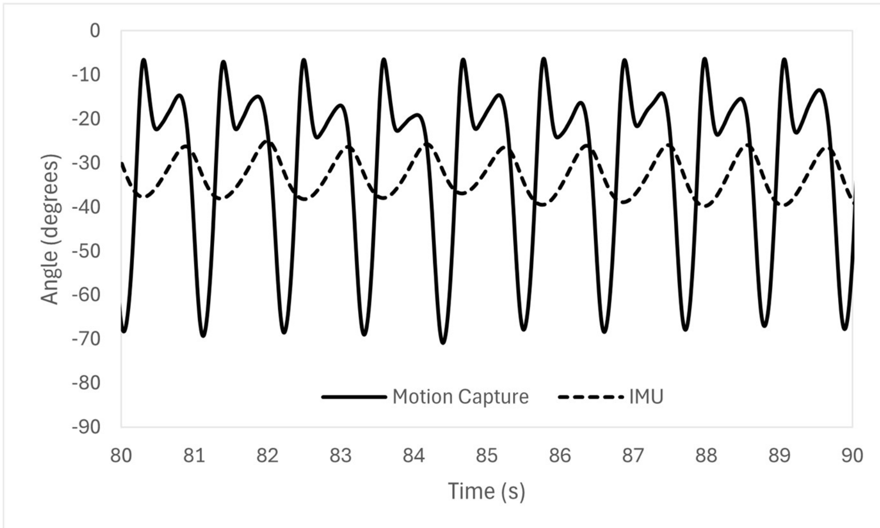

Figure 7. Sagittal knee joint angle during treadmill walking recorded using motion capture (solid) and calculated using gravitational acceleration measured by the IMUs at the thigh and shank (dashed). Nine strides are shown in the figure.

5.0 PHASE 2

5.1 METHODS

5.1.1 OVERVIEW OF PROTOCOL

Two pilot experiments and one main experiment were performed to validate the ability of a 'smart' brace, which was implemented with two SparkFun ICM-20948 IMUs to record knee kinematics. The first pilot experiment, called Wooden Rig Validation, involved affixing SparkFun IMUs and infrared reflective markers to a wooden, hinged rig to measure relative angles in a controlled environment. The second pilot experiment, called Xsens Validation, involved recording the right knee joint kinematics during a treadmill walking task using Xsens Awinda IMUs (Movella, Henderson, NV, USA), the 'smart' brace, and motion capture for a young, healthy participant. Finally, the main experiment, called ‘Smart’ Knee Brace Validation, involved recording the kinematics of the right knee joint using the ‘smart’ knee brace and motion capture for young, healthy participants during a variety of everyday movements. A sensor fusion algorithm found in MATLAB was used to calculate the relative knee joint angles between the SparkFun IMUs in all three protocols.

5.1.1.1 WOODEN RIG VALIDATION PROTOCOL

The SparkFun IMUs on the ‘smart’ brace were affixed to a wooden, hinged rig to test the validity of the IMUs and sensor fusion algorithm in measuring relative angles in a controlled setting. The rig was made to simulate a knee joint and was made of three wooden planks, a wooden base, and a 3D-printed hinge, as shown in Figure 8. The researcher affixed infrared reflective markers along with the SparkFun IMUs to the rig and positioned it in the motion capture collection space. The horizontal plank was referred to as the thigh plank and the vertical plank attached below the hinge was referred to as the shank plank when reflective markers were placed on the wooden rig. The thigh and shank planks were in a 90 degree orientation to each other when the rig was stationary and at rest. Since the thigh plank was fixed to the base while the shank plank was able to hinge, the shank plank was physically manipulated to resemble different angles of knee joint position. A total of five different trials were conducted using the rig and each trial was performed twice. In the first trial, the shank plank was kept at rest for 10 seconds, then rotated 90 degrees and held static for an additional 10 seconds to simulate a fully extended knee joint, before being returned to the rest position for another 10 seconds. In the second trial, the shank plank was kept at rest for 10 seconds, then rotated 90 degrees and back ten consecutive times, before being returned to the rest position for another 10 seconds. In the third trial, the shank plank was kept at rest for 10 seconds, rotated 90 degrees and held static for

10 seconds, tilted as far medial as the rig allowed, which was approximately 10 degrees, and held static for 10 seconds to mimic knee abduction, tilted as far lateral as the rig allowed, which was approximately 15 degrees, and held static for 10 seconds to mimic knee adduction, brought back to be collinear with the top plank and held static for 10 seconds, before being returned to the rest position for the final 10 seconds. Considering the experiments completed in Phase 1, it was realized that the axes of the IMUs at the thigh and shank were not perfectly aligned with the thigh and shank bone when the 'smart' brace was worn by an individual due to muscle and fat mass. This axis misalignment was simulated to investigate its effects on calculating relative angles with sensor fusion. To simulate the axis misalignment, two 1-inch by 5-inch strips of masking tape were rolled up and wedged under the top of the IMU on the thigh plank and under the bottom of the IMU on the shank plank. The wedges caused the IMUs to be angled approximately 10 to 20 degrees relative to the planks. The fourth and fifth trials were performed the same way as the second and third trials, respectively, but with the wedges placed under the IMUs.

5.1.1.2 XSENS VALIDATION PROTOCOL

The SparkFun IMUs on the 'smart' brace were validated against Xsens IMUs and the Vicon system, which are gold standard IMU and motion capture systems, respectively, for measuring knee joint angles during gait. Data were gathered using all three systems while a healthy, young, male participant (age = 26 years, mass = 68.2 kg, height = 1.73 meters) walked on the treadmill. The participant wore the 'smart' brace on the right leg and Xsens IMUs were bilaterally strapped to their lower limbs using Velcro, in the positions shown in Figure 9. The researcher then placed reflective markers on strategic anatomic locations on the participant's lower body for motion capture, as shown in Figure 2 and Table 1. The participant then performed one trial of treadmill walking during which they stood still on the treadmill for 10 seconds, walked at a comfortable, self-selected speed for 90 seconds, then stood still for another 10 seconds after the treadmill belt had come to a full stop.

5.1.1.3 'SMART' KNEE BRACE VALIDATION PROTOCOL

In this experiment, the 'smart' brace and motion capture recorded right knee joint kinematics while participants performed a variety of everyday movements. Participants visited the Biomechanics Lab at York University for two sessions with each lasting 1.5-2 hours. Participants were asked to wear skin-tight pants or shorts and wore the same attire for both sessions. Participants completed an informed voluntary consent and screening form at the beginning of the first session; basic anthropometric information such as age, height, weight, sex, and shank and thigh length were recorded. The protocol for 'Smart' Knee Brace Validation was identical to the protocol in Phase 1, except 15 squats and alternating leg lunges were completed for each of the squatting and lunging trials, respectively, instead of 10. The second session was identical to the first, taking place at least 24 hours later; anthropometric data were not collected and the PWS test was not conducted during the second session. Only data from the walking trials were analyzed for the purpose of this thesis. The walking, squatting, lunging, sit-to-stand, and jogging data were stored in York University's Dataverse to be used by students in the Lassonde School of Engineering for machine learning purposes.

5.1.2 INFORMED CONSENT AND PARTICIPANTS

A total of ten participants drawn from the general York University community volunteered for this study, but one met the exclusion criteria, leaving nine participants (five males and four females, age = 23.9 ± 2.1 years, mass = 70.9 ± 15.0 kg, height = 1.72 ± 0.1

meters). Participants provided written informed consent prior to testing and were assigned a random individual 2-digit code number. All data files were marked only with the corresponding code numbers to protect participant identity. Exclusion criteria included any history of neurological disorders, recent history (within the past 6 months) of musculoskeletal disorders, injuries, or significant pain. Inclusion criteria included generally good health, between the ages of 18 and 40 years of age, and the ability to both walk and jog unassisted for periods of at least 10 minutes.

5.1.3 EQUIPMENT AND MEASURES

5.1.3.1 WOODEN RIG VALIDATION & XSENS VALIDATION EQUIPMENT

The motion capture system, ‘smart’ brace, and treadmill used in the Wooden Rig Validation and Xsens Validation experiments were identical to the ones used in the protocol of Phase 1. The Wooden Rig Validation experiment utilized a hinged rig which was created by students in the Lassonde School of Engineering to simulate a knee joint and consisted of three wooden planks, a wooden base, and a 3D-printed hinge, as shown in Figure 8. The vertical and horizontal plank that was attached to the base remained fixed, while the vertical plank attached to the 3D-printed hinge was able to rotate, simulating knee flexion/extension and a small degree of adduction/abduction, but no internal/external rotation. A total of eight reflective markers were placed on the rig, using double-sided adhesive tape, for motion capture. Markers were placed on opposite sides of the rig, in both the proximal and distal positions of the horizontal plank to create a thigh segment in motion capture. The same was done for the plank attached below the hinge to create a shank segment. The horizontal plank was referred to as the thigh plank and the vertical plank attached below the hinge was referred to as the shank plank. Velcro strips were used to attach the SparkFun IMUs to both the thigh and shank planks, in the same relative locations they would be in if the 'smart' brace were worn by an individual.

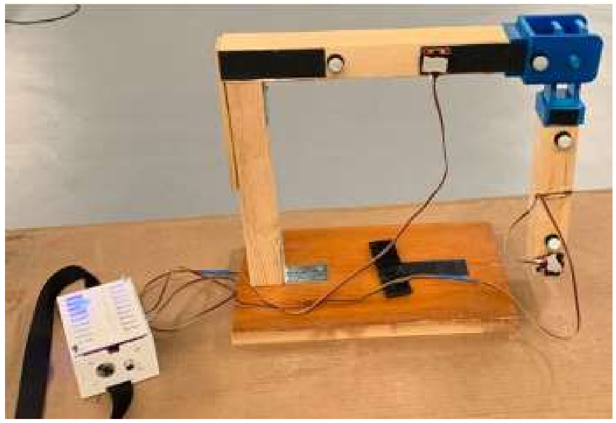

Figure 8: Hinged rig made to simulate a human leg. The blue component was made of 3D-printed material and contained the hinging mechanism, which allowed the rig to move like a knee joint. Four reflective markers were placed in a rectangular formation, using double-sided tape, on the horizontal plank of the hinge to simulate a thigh segment for 3D kinematics. Additionally, four more markers were placed in a rectangular formation on the vertical plank attached below the hinge to simulate a shank segment. The SparkFun IMUs from the 'smart' brace were placed on the rig in the same relative positions as were on the brace.

The Xsens Validation experiment used seven Xsens Awinda IMUs strapped bilaterally to each thigh, shank, foot, and one on the sacrum, as shown in Figure 9; data were sampled at 100 Hz. The Xsens IMUs on the right thigh and shank were placed directly on top of the SparkFun IMUs at the thigh and shank, respectively, on the 'smart' brace. The same motion capture system, 'smart' brace, and treadmill that was used in Phase 1 was also used in this experiment.

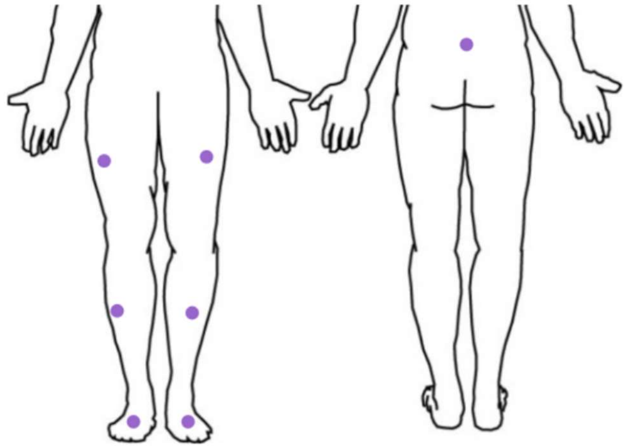

Figure 9: Seven Xsens IMUs were bilaterally placed on the thighs, shanks, feet, and one on the sacrum. The Xsens IMU on the right thigh and shank were placed directly on the right thigh and shank SparkFun IMUs on the 'smart' brace, respectively.

5.1.3.2 'SMART' KNEE BRACE VALIDATION EQUIPMENT AND MEASURES

The equipment used in the protocol for 'Smart' Knee Brace Validation was identical to the equipment in Phase 1. Individual anthropometrics such as height and weight were measured using a weight scale (Seca, Chino, CA, USA), while a measuring tape was used to measure each participant's thigh and shank length. Both motion capture and the 'smart' brace were used to collect right knee joint parameters such as knee extension angle during heel strike, maximum flexion, maximum adduction, maximum abduction, maximum internal, and maximum external rotation angles, as well as sagittal, frontal, and axial plane ranges of motion.

5.1.4 DATA PROCESSING

5.1.4.1 WOODEN RIG VALIDATION DATA PROCESSING

Motion capture data were filtered in MATLAB using a 4^{th} order low-pass Butterworth filter with a cut-off frequency of 4 Hz, which was based on a residual analysis (Winter, 2009). The SparkFun IMU data were filtered in MATLAB using a 4^{th} order low-pass Butterworth filter with a cut-off frequency of 2 Hz, based on a residual analysis (Winter, 2009), before being interpolated to 100 Hz, using the interp1() function in MATLAB, to match the motion capture sampling rate. After the raw IMU data were filtered and interpolated, accelerometer data were converted from milli-g's to meters/second^2, and gyroscope data were converted from degrees/second to radians/second. An AHRS filter in MATLAB was used for sensor fusion of the SparkFun IMUs. Since the AHRS filter calculated the orientation of each IMU as an absolute angle in the three planes of movement, the orientation of the IMU at the thigh plank was subtracted by the orientation of the IMU at the shank plank to obtain the relative angles between the thigh and shank planks (Winter, 2009). This method was used for the sagittal and frontal planes to obtain the flexion/extension and adduction/abduction relative knee angles, respectively. The relative angles measured by the motion capture system between the thigh and shank segments on the wooden rig were calculated using the dot product method, as shown in (3). The positions of the two markers positioned at each end of the thigh segment were averaged to form the initial point and end point of the thigh vector. The same protocol was used for the markers on the shank plank to create a shank vector. Equation (3) was then used to calculate the relative angles between the thigh and shank vectors in the sagittal and frontal planes:

$$\theta = cos^{-1}(\frac{a \cdot b}{|a||b|}) \tag{3}$$

Where a and b are the thigh and shank vectors, respectively.

5.1.4.2 XSENS VALIDATION DATA PROCESSING

Motion capture data were filtered in Visual3D using a 4th order low-pass Butterworth filter with a cut-off frequency of 6Hz (Winter, 2009). The SparkFun IMU data were filtered in MATLAB using a 4th order low-pass Butterworth filter with cut-off frequencies based on a residual analysis (Winter, 2009), before being interpolated to 100 Hz, using the interp1() function in MATLAB, to match the motion capture sampling rate. The accelerometer, gyroscope, and magnetometer data in the X, Y, and Z axes of the SparkFun IMU at the thigh were filtered with cut-off frequencies of 4 Hz, 4 Hz, 4 Hz, 4 Hz, 5 Hz, 4 Hz, 3 Hz, 3 Hz, and 3 Hz, respectively. The accelerometer, gyroscope, and magnetometer data in the X, Y, and Z axes of the SparkFun IMU at the shank were filtered with cut-off frequencies of 5 Hz, 4 Hz, 5 Hz, 4 Hz, 4 Hz, 4 Hz, 4 Hz, 3 Hz, and 4 Hz, respectively. As was done in the Wooden Rig Validation experiment, accelerometer and gyroscope data were converted to meters/second^2 and radians/second, respectively, and the AHRS filter in MATLAB was used to calculate right knee flexion/extension, adduction/abduction, and internal/external rotation angles. Sensor fusion of the Xsens IMUs were achieved using Xsens' proprietary Xsens Kalman Filter for 3 degrees-of-freedom orientation for Human Motion (XKF3hm). Once the knee joint angles from the SparkFun IMUs were calculated, the biases of the knee joint angles obtained while the participant was standing quietly at the very beginning of each trial were calculated by calculating the average of the first 10 to 15 seconds of every trial, for each of the motion capture, Xsens, and 'smart' brace signals, and in all three planes of motion. The differences between the biases of the motion capture to each of the Xsens and 'smart' brace knee joint angles were then added to the signal of each respective system to align the Xsens and 'smart' brace signals to the motion capture signal, for all three planes of motion. Positive angles represented knee extension, abduction, and internal rotation, while negative angles represented knee flexion, adduction, and external rotation, for the Xsens Validation and 'Smart' Knee Brace Validation experiments.

5.1.4.3 ‘SMART’ KNEE BRACE VALIDATION DATA PROCESSING

Motion capture and SparkFun IMU data were processed as was done in the Xsens Validation experiment. As was done in the Wooden Rig Validation and Xsens Validation experiments, the AHRS filter from MATLAB was used for sensor fusion and the right knee flexion/extension, adduction/abduction, and internal/external rotation angles were calculated. The motion capture and ‘smart’ brace signals in all three planes of motion were aligned, as was done in the Xsens Validation experiment. Ensemble curves were generated by averaging the right knee joint angle waveforms from ten consecutive strides in each trial, normalized from heel contact to heel contact. Right knee joint parameters were obtained for each of the ten consecutive strides and averaged for each trial.

5.1.5 STATISTICAL ANALYSES

Data from the Wooden Rig Validation and Xsens Validation experiments were visually compared; no statistical tests were performed. Statistical analyses for the ‘Smart’ Knee Brace Validation experiment were performed using SPSS (Version 29, IBM Corporation, Armonk, NY, USA) and JMP (Version 17.2.0, JMP Statistical Discovery LLC, Cary, NC, USA), with an alpha of 0.05 used throughout all the analyses to indicate statistical significance. All data samples were tested for normality using the Shapiro-Wilk test of normality before further statistical tests were performed. Positively skewed datasets were corrected using a log transform, while data which were negatively skewed were reflected and then log transformed. Outliers were identified through box and whisker plots and values not within two standard deviations of the mean were removed from further analysis. A cross-correlation was performed in JMP to analyze the similarity between the time series knee joint angle signals in the three planes of motion, at zero lag, for the motion capture system and the ‘smart’ brace. Bland-Altman plots with 95% limits of agreement (LOA) were created in Excel (Version 2403, Microsoft Corporation, Redmond, WA, USA) to assess agreement between the motion capture system and the ‘smart’ brace for each measure by using the mean of all walking trials for each participant, for each system. An intraclass correlation (ICC) test (3, k = 3) was used to assess the test-retest reliability between sessions, for both systems. ICC values of < 0.5, 0.5-0.75, 0.75-0.9, and > 0.9 were indicative of poor, moderate, good, and excellent reliability, respectively (Koo and Li, 2016). A two-way repeated measures analysis of variance (ANOVA) was also performed in JMP for each dependent measure. The error term was comprised of the factor “Trial” nested within the factor “Participant”. The two within-subjects factors, SYSTEM and SESSION, each had two levels: motion capture and ‘smart’ brace, and session 1 and session 2, respectively. A Wilcoxon signed rank test was performed when an interaction effect was present to assess which group means were significantly different from each other.

5.2 RESULTS

5.2.1 WOODEN RIG VALIDATION RESULTS

Upon visual inspection of the simulated flexion/extension rotations of the wooden rig in Figure 10, it was observed that while the motion capture system measured maximum extension angles approximately 10 degrees larger than those calculated by the SparkFun IMUs, the relative angles measured when the wooden rig was kept in a static state were nearly identical. This 10-degree difference between the motion capture system and SparkFun IMUs was also observed for the trials where the shank plank was rotated 90 degrees ten consecutive times with a wedge placed under each of the SparkFun IMUs.

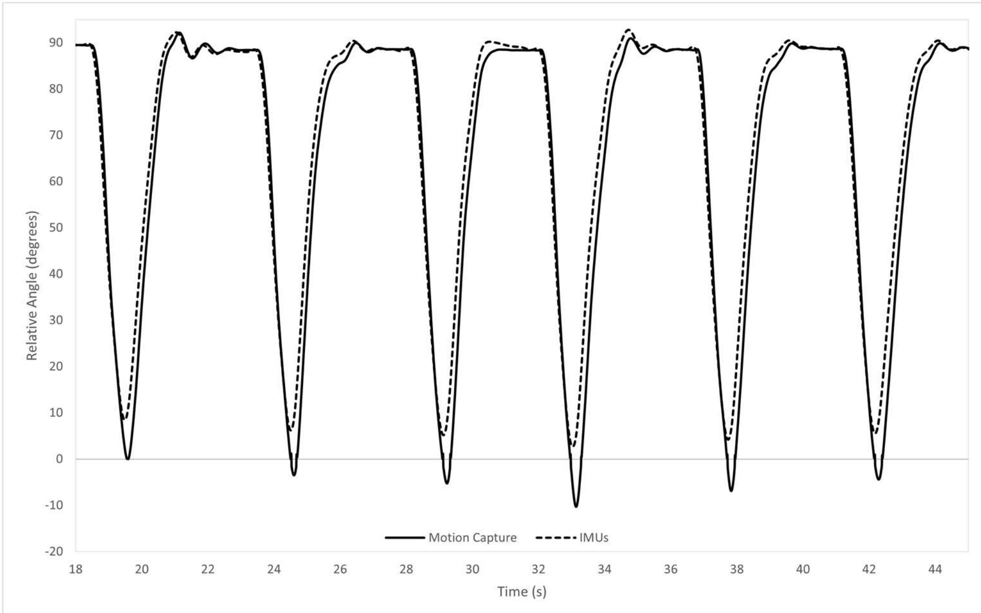

Figure 10. The relative angles measured between the thigh and shank plank of the wooden rig when simulating the flexion/extension movements of a knee joint for the motion capture system (solid) and SparkFun IMUs (dotted). These were the calculated angles for the trial where the shank plank was kept at rest for 10 seconds, rotated 90 degrees from the resting position and back ten consecutive times, before being brought back to the rest position for another 10 seconds, without a wedge placed under the IMUs. Only six of the ten rotations are shown in the figure.

Upon visual inspection of the simulated abduction/adduction rotations of the wooden rig in Figure 11, it was observed that the motion capture system measured maximum abduction or adduction angles that were approximately 2 to 4 degrees larger than the angles calculated by the SparkFun IMUs. The 2-to-4-degree difference was also seen for the abduction/adduction trials where a wedge was not placed under the IMUs on the thigh and shank planks.

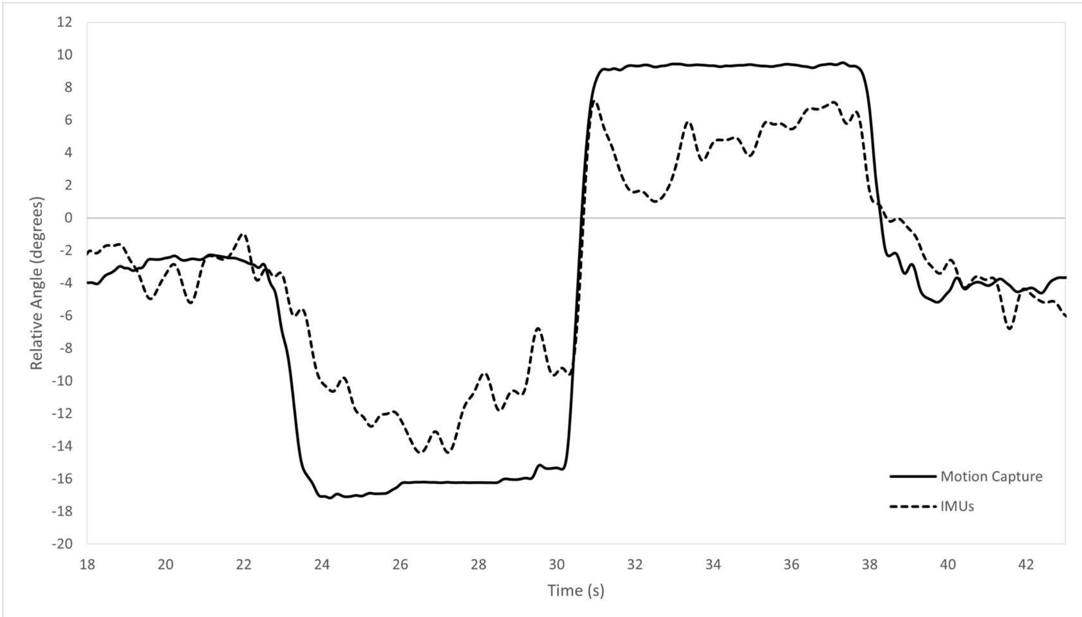

Figure 11. The relative angles measured between the thigh and shank plank of the wooden rig when simulating the abduction/adduction movements of a knee joint for the motion capture system (solid) and SparkFun IMUs (dotted). A wedge was placed under the top of the IMU on the thigh plank and under the bottom of the IMU on the shank plank for this trial. The figure shows when the shank plank was held collinear with the thigh plank and static for 10 seconds, tilted as far medial as the rig allowed for 10 seconds, tilted as far lateral as the rig allowed for 10 seconds, and brought back to be collinear with the thigh plank and held static for 10 seconds.

5.2.2 XSENS VALIDATION RESULTS

Upon visual inspection of the graphs in Figure 12, it was observed that although the shape of the ‘smart’ brace signals were similar to the Xsens signals in all three planes, the amplitude of the ‘smart’ brace signal was much larger than the Xsens signal in the frontal plane and contained a bias in the sagittal plane even after the signals were aligned at the beginning of the trial, when the participant was quietly standing. The ‘smart’ brace and Xsens signals both had a bias in the frontal and axial planes when compared to the motion capture signals. The shape and amplitude of the Xsens signals were very similar to the motion capture signals in all three planes.

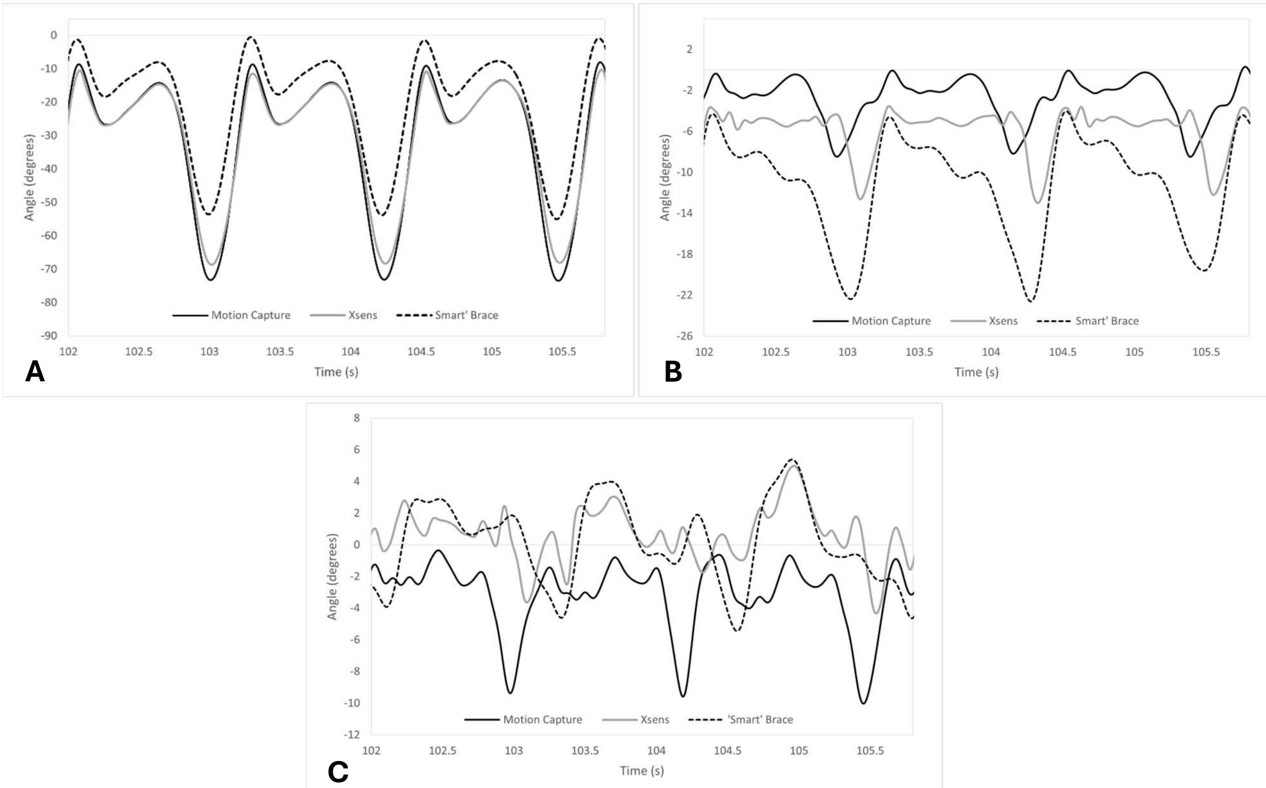

Figure 12. Right knee joint angle in the (A) sagittal, (B) frontal, and (C) axial planes during a trial of treadmill walking recorded by the motion capture system (solid black), Xsens system (solid grey), and the ‘smart’ knee brace (dotted black). Three strides approximately from heel contact to heel contact are shown in the figures.

5.2.3 ‘SMART’ KNEE BRACE VALIDATION RESULTS

Cross-correlation of the sagittal right knee angle signals in Figure 13 A indicated that the motion capture system and ‘smart’ brace had a strong positive relationship ($\rho = 0.996$, $p < 0.001$, df = 99). The signals of axial knee angle in Figure 13 B also had a strong positive relationship ($\rho = 0.795$, $p < 0.001$, df = 99), but the ‘smart’ brace signal had standard deviations that were larger than its amplitude. The signals of frontal knee angle in Figure 13 C had a weak relationship ($\rho = 0.048$, $p = 0.63$, df = 99) and the standard deviation of the ‘smart’ brace signal was also larger than its amplitude.

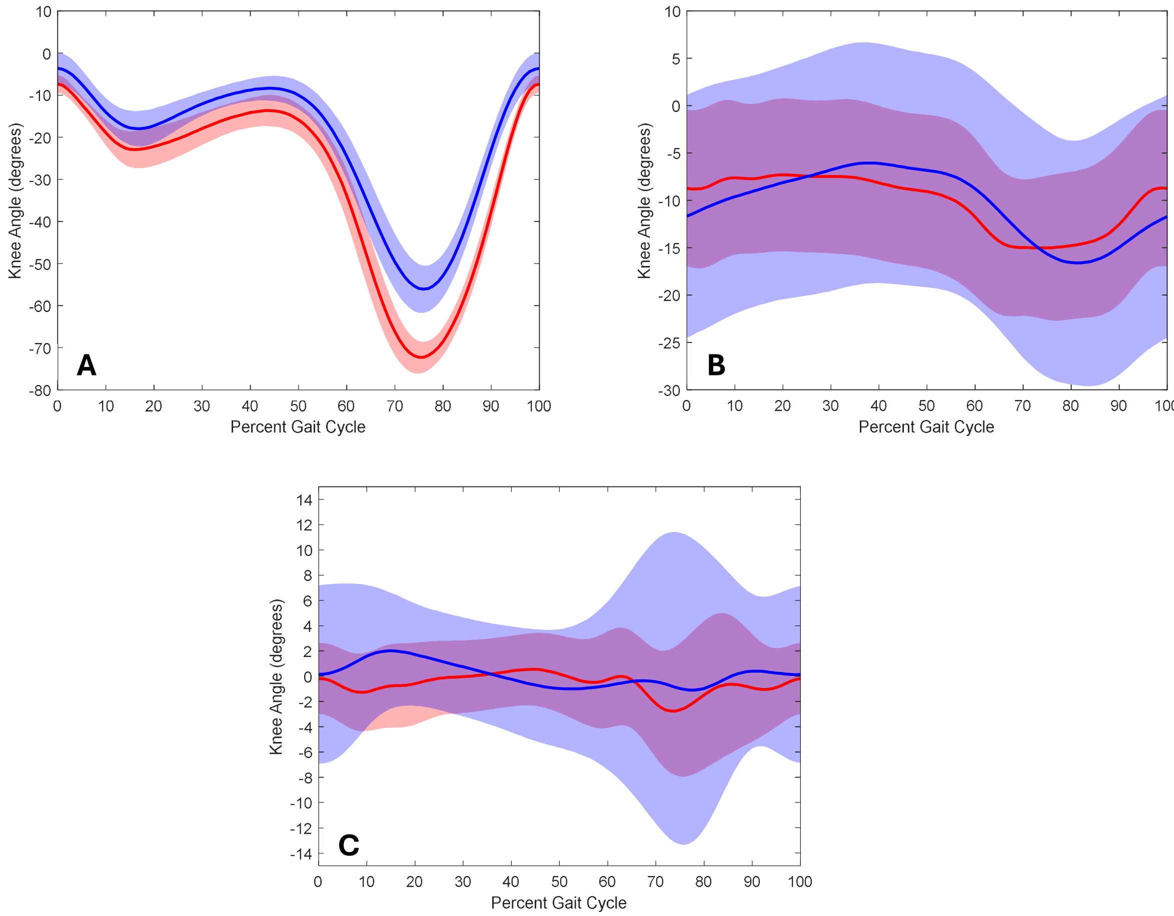

Figure 13. Ensemble average and standard deviation of the right (A) sagittal, (B) axial, and (C) frontal knee joint angles, normalized to one gait cycle from heel contact to heel contact, for ten strides of treadmill walking per trial, from all participants for the motion capture system (red) and ‘smart’ brace (blue).

BA plots from Figure 14 and Table 2 showed that the biases for the dependent measures between the motion capture system and ‘smart’ brace ranged from 0.43 to 16.19 degrees. The plots in Figure 14 showed that the ‘smart’ brace underestimated sagittal plane range of motion, maximum external rotation, and maximum adduction angles compared to the motion capture system. The ‘smart’ brace overestimated the knee extension angle during heel strike, maximum flexion, internal rotation, and abduction angles, as well as axial and frontal plane range of motion compared to the motion capture system. Motion capture data were excluded for maximum knee adduction, abduction, and axial range of motion for Participant 6, and maximum knee internal rotation for Participant 5 due to the prevalence of multiple outliers in those datasets. The exclusion of these data can be seen in Figure 14 indicated by the presence of eight dots in the BA plots for maximum knee adduction, abduction, internal rotation, and axial range of motion instead of nine.

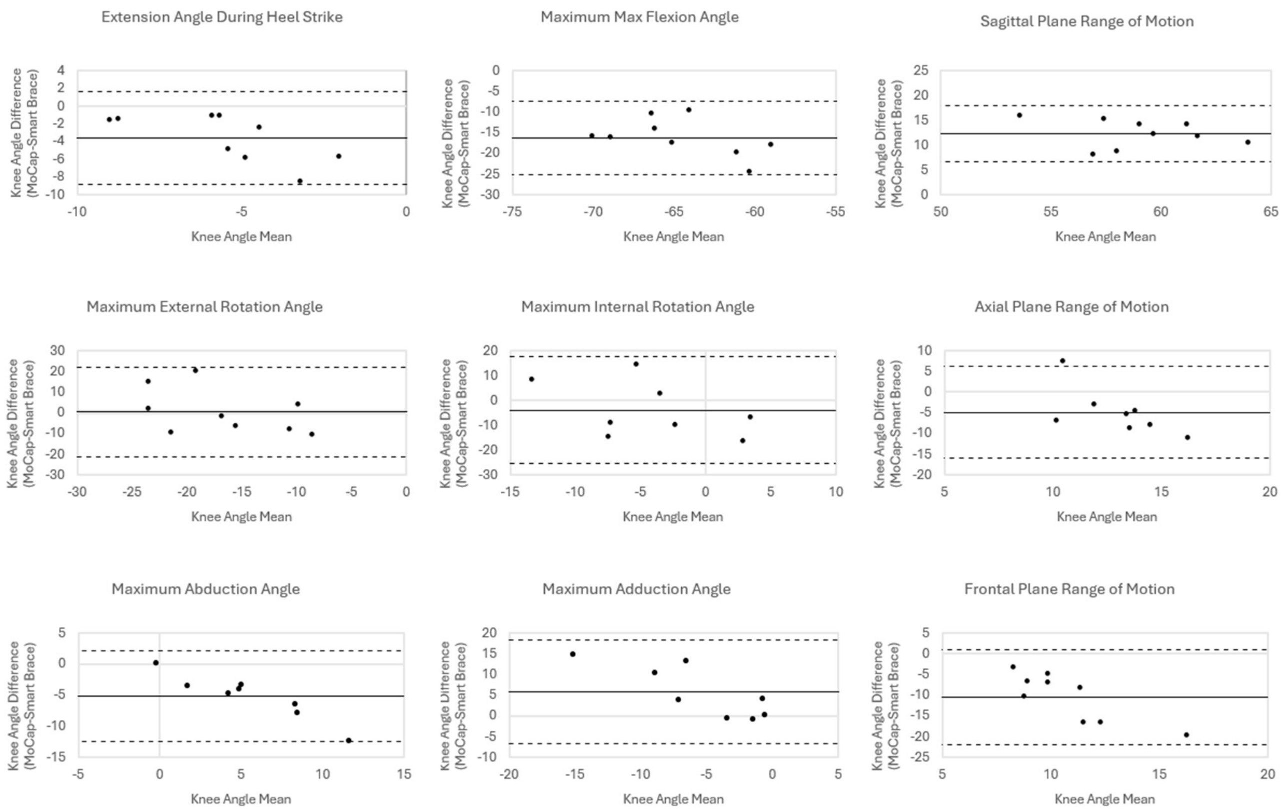

Figure 14. Bland-Altman (BA) plots with 95% limits of agreement (LOA) for all dependent measures between the motion capture system and 'smart' brace. The solid black line represents the bias, the dotted black lines represent the 95% LOA, and the black circles represent the average of ten strides, from all trials, from each participant (n = 9). A positive bias indicates an underestimation, and a negative bias indicates an overestimation of the 'smart' brace compared to the motion capture system.

As shown in Table 2, the motion capture system demonstrated moderate to excellent reliability for all dependent measures except maximum internal rotation angle (0.280) and axial plane range of motion (0.444). However, maximum external rotation, internal rotation, axial, and frontal plane range of motion were not significant. The 'smart' brace demonstrated moderate to excellent reliability for all measures except for maximum external (0.489) and internal (0.331) rotation angles. However, maximum external rotation, internal rotation, and frontal plane range of motion were not significant. As shown in Table 2 and Figure 15, there was a significant interaction effect for maximum flexion angle [$F(1,8) = 7.366$, $p = 0.026$]. Post-hoc Wilcoxon signed rank tests between the group means for maximum flexion angle showed statistically significant differences between 'smart' brace session 1 and 'smart' brace session 2 ($Z = -2.895$, $p = 0.004$), MoCap session 1 and 'smart' brace session 1 ($Z = -4.541$, $p < 0.001$), MoCap session 1 and 'smart' brace session 2 ($Z = -4.541$, $p < 0.001$), MoCap session 2 and 'smart' brace session 1 ($Z = -4.541$, $p < 0.001$), and MoCap session 2 and 'smart' brace session 2 ($Z = -4.541$, $p < 0.001$). There was a significant main effect of SYSTEM for the extension angle during heel strike [$F(1,8) = 8.914$, $p = 0.010$], maximum flexion [$F(1,8) = 69.355$, $p < 0.0001$], and sagittal [$F(1,8) = 85.173$, $p < 0.0001$] and frontal [$F(1,8) = 31.970$, $p < 0.0001$] plane range of motion. There was a significant main effect of SESSION for maximum abduction angle [$F(1,8) = 6.484$, $p = 0.046$].

Table 2. Test-retest reliability (ICC(3, k)), bias, 95% LOA, and two-way repeated measures ANOVA p-values for the interaction effect, main effect of SYSTEM, and main effect of SESSION. Statistically significant differences (p <0.05) are indicated by an asterisk (*).

Measure	ICC(3, k = 3)		Motion Capture Vs 'Smart' Brace			
				Two-way RMANOVA		
	MoCap	'Smart' Brace	Bias (95% LOA)	SYSTEM	SESSION	SYSTEM x SESSION
Extension Angle During Heel Strike	0.778*	0.860*	-3.62 (-8.87, 1.64)	p = 0.010*	p = 0.176	p = 0.181
Maximum Flexion Angle	0.845*	0.727*	-16.19 (-25.07, -7.32)	p = <0.0001*	p = 0.283	p = 0.026*
Sagittal Plane Range of Motion	0.909*	0.835*	12.36 (6.75, -17.96)	p = <0.0001*	p = 0.711	p = 0.090
Maximum External Rotation Angle	0.506	0.489	0.43 (-21.13, 21.99)	p = 0.672	p = 0.125	p = 0.933
Maximum Internal Rotation Angle	0.280	0.331	-4.02 (-25.57, 17.52)	p = 0.551	p = 0.095	p = 0.919
Axial Plane Range of Motion	0.444	0.943*	-4.92 (-15.96, 6.11)	p = 0.135	p = 0.403	p = 0.540
Maximum Abduction Angle	0.801*	0.643*	-5.14 (-12.38, 2.09)	p = 0.056	p = 0.046*	p = 0.122
Maximum Adduction Angle	0.816*	0.889*	5.75 (-6.72, 18.21)	p = 0.135	p = 0.258	p = 0.986
Frontal Plane Range of Motion	0.657	0.599	-10.42 (-21.85, 1.01)	p = <0.0001*	p = 0.119	p = 0.154

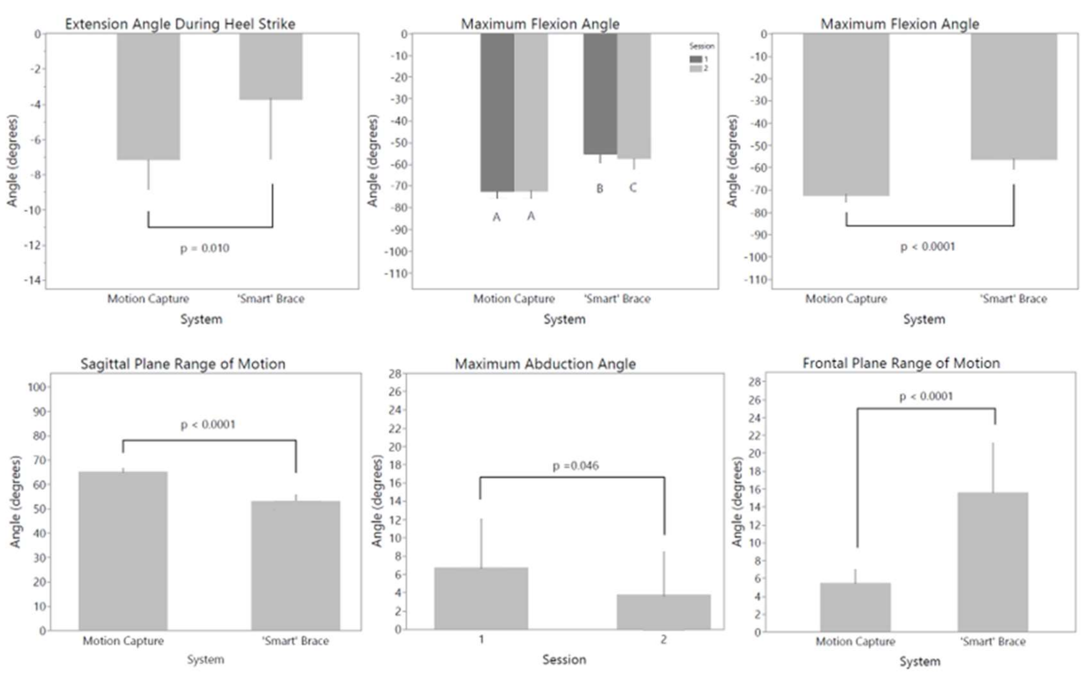

Figure 15. Maximum flexion angle had a significant interaction effect and post-hoc Wilcoxon signed rank tests showed that all pairwise comparisons for maximum flexion angle were

significantly different except for MoCap session 1 and MoCap session 2. Bars with matching letter pairs were not significantly different from each other. Extension angle during heel strike, maximum flexion angle, sagittal plane range of motion, and frontal plane range of motion had a significant main effect for SYSTEM, while maximum abduction angle had a significant main effect for SESSION.

5.3 DISCUSSION

The aim of this thesis was to examine the agreement and reliability of an IMU-instrumented ‘smart’ brace in comparison with a gold standard optoelectronic motion capture system. It was hypothesized that the ‘smart’ brace would be reliable across multiple testing sessions and agree with the motion capture system in measuring knee joint angles during treadmill walking. The results of Phase 1 did not support the hypothesis because the coordinate axes of the SparkFun IMUs did not align with the coordinate axes of the motion capture system, which made it difficult to compare signals between the two systems. Phase 2 utilized a sensor fusion algorithm that allowed knee joint angles to be calculated using data collected from the IMUs, which were then compared to the knee joint angles derived from a motion capture system. The results of the ‘Smart’ Knee Brace Validation experiment from Phase 2 partially supported the hypothesis such that the ‘smart’ brace had moderate to excellent reliability in measuring knee joint angles in the sagittal and frontal plane but had poor reliability in measuring maximum knee rotation angles in the axial plane. The results of the analysis of variance and the Bland-Altman plots showed that the ‘smart’ brace was not in agreement with the motion capture system in measuring knee angles in the sagittal plane and the frontal plane range of motion.

5.3.1 PHASE 1 DISCUSSION

Phase 1 of this thesis focused on validating the accelerometers and gyroscopes of the IMUs on the ‘smart’ brace against the motion capture system. Upon visual inspection of the signals collected or calculated from the Linear Accelerations of Plate Centroid experiment, the periodicity of linear acceleration signals of the IMUs was similar to the linear acceleration of the centroid of the markers on the plates attached to the thigh and shank IMUs in the Y and Z axes. However, the X, Y, and Z coordinate axes of the IMUs were not perfectly aligned with the X, Y, and Z coordinate axes of the motion capture space. This misalignment was due to the coordinate axes of the IMU constantly changing along with the orientation of the IMU, while the coordinate axes of the motion capture system remained fixed from the initial calibration of the motion capture space. For the Vector Sum of Accelerations experiment, the periodicity of the signals of vector sum of accelerations from the two systems were similar, but based upon visual inspection, the IMUs on the 'smart' brace were unable to match the quick fluctuations seen during the peaks and troughs of the vector sum signal for the motion capture system. In the Angular Velocities of Plate experiment, the angular velocities of the gyroscopes from the IMUs in the antero-posterior and longitudinal axes did not produce similar peaks or troughs as the angular velocities of the LCSs of the plates attached to the thigh and shank IMUs, based upon visual inspection. The marker position data from the motion capture system was heavily processed and differentiated to calculate marker acceleration and LCS angular velocity, which may have introduced higher-frequency noise into the signals of the vector sum of triaxial acceleration of the marker on the thigh and shank IMU and angular velocity of the LCSs of the plates attached to the IMUs, respectively (Winter, 2009). Finally, the Gravitational Acceleration Angle experiment was unable to calculate knee joint angles similar to those obtained by the motion capture system using the acceleration of gravity sensed by the accelerometers. The pitch and roll orientation of an IMU can be calculated using gravitational acceleration when the IMU is in a static state, but during gait, the movement of the lower limbs introduced too much linear acceleration to accurately estimate the IMU's orientation (Nazarahari & Rouhani, 2021). In summary, the direct output of the accelerometers and gyroscopes of the IMUs were not comparable to those of the motion capture system. This discrepancy may have been due to difficulties in aligning the coordinate axes of the IMUs with those of the motion capture system, the extensive processing of motion capture data needed for one-to-one comparisons with IMU data, which reduced the signal-to-noise ratio, and the dynamic nature of walking, which introduced too many external accelerations to accurately estimate the IMUs' sagittal orientation.

5.3.2 WOODEN RIG VALIDATION & XSENS VALIDATION DISCUSSION

Since it was difficult to compare the direct outputs of the accelerometers and gyroscopes to the gold standard motion capture system, a sensor fusion algorithm was implemented in Phase 2 of this thesis. The AHRS filter used in MATLAB is a type of sensor fusion algorithm that allows researchers to calculate knee joint angles by integrating the linear acceleration, angular velocity, and magnetic field data collected from the IMUs. The Wooden Rig Validation experiment in Phase 2 of this thesis found that the adduction/abduction angles calculated using the data collected by the SparkFun IMUs were very similar to the motion capture system when measuring the relative angle between the two planks of the wooden rig. The flexion/extension angles calculated from the IMU data were more comparable to the motion capture system during the static portions of the trial compared to the dynamic portions. For the Xsens Validation experiment, the knee joint angle signal from the 'smart' brace continued to show a bias, even after the 'smart' brace, Xsens, and motion capture signals were aligned for all three planes of movement. The shape and periodicity of the 'smart' brace signals were similar to the Xsens system in all three planes, but based upon visual inspection, the amplitudes of the 'smart' brace were larger in the frontal plane and smaller sagittal plane. In summary, the Wooden Rig

Validation experiment found that the relative angles calculated using SparkFun IMU data in a controlled and static setting were similar to a gold standard optoelectronic motion capture system. The Xsens Validation experiment found that the knee angles calculated using data collected from the 'smart' brace were similar to the Xsens system but had difficulty measuring accurate sagittal and frontal knee ranges of motion.

5.3.3 'SMART' KNEE BRACE VALIDATION DISCUSSION

The 'Smart' Knee Brace Validation experiment found that the 'smart' brace had poor to moderate agreement in calculating knee joint angles using data collected from the IMUs on the brace compared to the motion capture system, and moderate to excellent reliability in the sagittal and axial planes. The correlation coefficient between the 'smart' brace and motion capture system that was found for the sagittal right knee angle was similar to previous studies, which all had coefficients above 0.85 during overground walking (Favre, Jolles, Aissaoui, & Aminian, 2008; Takeda, Tadano, Natorigawa, Todoh, & Yoshinari, 2009; Cloete & Scheffer, 2008). The study done by Favre et al. (2008) reported higher correlation coefficients for axial and frontal knee angles with values of 0.95 and 0.86, respectively, compared to 0.795 and 0.048 found in the current study. This difference could be attributed to their IMUs being placed on a rigid plastic plate and securely strapped to the thigh and shank, reducing skin artifacts.

Previous studies found that IMU systems overestimated sagittal knee range of motion compared to a 3D motion capture system and had biases that were less than 5 degrees (Al-Amri et al., 2018; Bell et al., 2019; Zügner et al., 2019). This overestimation is in stark contrast to the 'smart' brace, which underestimated sagittal plane range of motion with a bias of 12.36 degrees compared to the motion capture system. However, it should be noted that the studies done by Bell et al. (2019) and Zügner et al. (2019) analyzed knee joint angle during a sit-to-stand movement and included older adults who had undergone total hip arthroplasty within the past two to five years, respectively. A previous study comparing DorsaVi IMUs to a Vicon motion capture system during overground walking in patients with knee osteoarthritis reported a similar bias between the two systems for knee extension during heel strike (Binnie et al., 2021). However, Binnie et al. (2021) found that their IMU system underestimated maximum knee flexion by about 3 degrees, whereas, in the current study, the 'smart' brace underestimated by 16.19 degrees. Al-Amri et al. (2018) found that their IMU system overestimated knee abduction and underestimated knee adduction by up to about 5 degrees, which is similar to what was found for the 'smart' brace, but underestimated frontal knee range of motion by about 5 degrees, whereas the 'smart' brace overestimated by 10.42 degrees. The overestimation of 10.42 degrees is large considering frontal knee range of motion for healthy individuals is approximately 10 degrees (Chao, Laughman, Schneider, & Stauffer, 1983).

The 'smart' brace demonstrated similar levels of reliability as the Xsens system used by Al-Amri et al. (2018) for all measures, except for maximum external rotation angle; the 'smart' brace showed poor reliability, but Xsens was excellent. The motion capture system was expected to have good to excellent reliability for all measures as it is considered the industry standard motion capture system but had poor to moderate reliability for maximum external rotation, maximum internal rotation, axial plane, and frontal plane range of motion. This discrepancy could be attributed to tissue artefacts and the 'smart' brace shifting up to 5 centimeters down the leg during and after every trial. The brace would be repositioned on the leg after every trial so that the reflective markers were once again, on anatomical landmarks.

The results of the two-way repeated measures ANOVA showed that the motion capture system measured larger angles than the 'smart' brace, and that the brace measured significantly different angles between sessions for the measure of maximum knee flexion. The interaction effect contradicts the results of the ICC test that reported good reliability for maximum flexion angle of the ‘smart’ brace. Although the ICC test reported poor reliability for the motion capture system and ‘smart’ brace in measuring maximum external and internal rotation angles, the two-way repeated measures ANOVA did not suggest that these measures differed significantly between days. The ‘smart’ brace was not accurate in measuring extension angle during heel strike, maximum flexion angle, and sagittal and frontal plane range of motion, as confirmed by the results of the ANOVA, which suggested that these measures differed significantly between systems.

There were numerous limitations that were encountered in this study. Although a small sample size was included, this study utilized an early adaptation of a novel ‘smart’ brace for research and development purposes, so achieving an adequate sample size was not the main objective. As previously mentioned, the ‘smart’ brace would shift up to 5 centimeters down a participant’s leg if flexion/extension movements were performed and would occur more frequently if a participant had shorter or skinnier legs. The repositioning of the brace on the participant’s leg would cause the reflective markers that were placed on anatomic locations on the brace to be sub-optimally positioned for 3D kinematics. The IMUs were positioned on the brace such that they would be situated at mid-thigh and mid-shank when the ‘smart’ brace was worn by a participant. This was not the case when participants with longer legs wore the ‘smart’ brace; due to its length, the IMU at the thigh would be positioned distal to the mid-point of the thigh. Finally, achieving consistent placement of the ‘smart’ brace on participants in the same location every session, or even before every trial, provides a challenge. Future studies could improve the results found in this thesis by exploring different types of fusion algorithms used to estimate IMU orientation. This could allow for more accurate and precise measurements of knee joint angle in the sagittal, frontal, and axial planes, especially during more dynamic movements. Additionally, a variety of compression sleeve sizes should be available for participants of different thigh and shank lengths to provide for optimal IMU placement. Finally, future studies should validate custom IMU systems against a gold standard IMU system in all three planes of movement. There would be a more direct comparison since the gold standard IMU could be placed directly on top of the custom IMU. Raw accelerometer, gyroscope, and magnetometer data could also be extracted from the gold standard IMU and integrated with the same sensor fusion algorithm applied to the custom IMU data to validate the algorithm being used.

6.0 CONCLUSION

In conclusion, this study aimed to assess the agreement and reliability of a novel 'smart' brace in comparison to a gold standard optoelectronic motion capture system for measuring knee joint angles during treadmill walking. Experiments in this study validating the direct outputs of the accelerometers and gyroscopes of the IMUs in the 'smart' brace to a motion capture system showed that a one-to-one comparison of linear accelerations and angular velocities between the two systems was not successful. The coordinate axes of the motion capture system remained fixed while the coordinate axes of the IMUs were constantly changing as the orientation of the IMU changed. Also, the processing of position data recorded from the motion capture system to angular velocity or vector sum of triaxial acceleration introduced too much noise to produce signals comparable to the IMUs. A sensor fusion algorithm integrating accelerometer, gyroscope, and magnetometer data to estimate the orientation of an IMU enabled the calculation of knee joint angles that were compared to those from a motion capture system. The 'smart' brace reported moderate to excellent reliability between sessions for knee angles in the sagittal plane, frontal plane, and axial plane range of motion. However, the joint angles measured in the sagittal plane and for the frontal plane range of motion were not in agreement with the motion capture system. Although the small sample size was a limitation, this study aimed to validate the first iteration of the ‘smart’ brace and sought to examine its capabilities in measuring knee kinematics. Other limitations included inconsistent brace placement between sessions and even trials, leading to inconsistent reflective marker and IMU placement on the lower limbs. Future studies could improve the results found from this study by exploring different sensor fusion algorithms for estimating IMU orientation, accommodating ‘smart’ brace sizes based on participant lower limb lengths, and by comparing custom IMU systems to gold standard IMU systems for a more direct comparison.

REFERENCES

Abid, M., Mezghani, N., & Mitiche, A. (2019). Knee Joint Biomechanical Gait Data Classification for Knee Pathology Assessment: A Literature Review. *Applied Bionics and Biomechanics*, 2019, 7472039–14. https://doi.org/10.1155/2019/7472039

Abulhasan, J., & Grey, M. (2017). Anatomy and Physiology of Knee Stability. *Journal Of Functional Morphology And Kinesiology*, 2(4), 34. doi: 10.3390/jfmk2040034

Ahn, J., & Hogan, N. (2012). Walking is not like reaching: evidence from periodic mechanical perturbations. *PloS One*, 7(3), e31767–. https://doi.org/10.1371/journal.pone.0031767

Al-Amri, M., Nicholas, K., Button, K., Sparkes, V., Sheeran, L., & Davies, J. L. (2018). Inertial Measurement Units for Clinical Movement Analysis: Reliability and Concurrent Validity. *Sensors* (Basel, Switzerland), 18(3), 719-. https://doi.org/10.3390/s18030719

Binnie, T., Smith, A., Kent, P., Ng, L., O'Sullivan, P., Tan, J.-S., Davey, P. C., & Campbell, A. (2022). Concurrent validation of inertial sensors for measurement of knee kinematics in individuals with knee osteoarthritis: A technical report. *Health and Technology*, 12(1), 107–116. https://doi.org/10.1007/s12553-021-00616-9

Bell, K. M., Onyeukwu, C., McClincy, M. P., Allen, M., Bechard, L., Mukherjee, A., Hartman, R. A., Smith, C., Lynch, A. D., & Irrgang, J. J. (2019). Verification of a Portable Motion Tracking System for Remote Management of Physical Rehabilitation of the Knee. *Sensors* (Basel, Switzerland), 19(5), 1021-. https://doi.org/10.3390/s19051021

Chao, E. Y., Laughman, R. K., Schneider, E., & Stauffer, R. N. (1983). Normative data of knee joint motion and ground reaction forces in adult level walking. *Journal of Biomechanics*, 16(3), 219–233. https://doi.org/10.1016/0021-9290(83)90129-X

Cloete, T., & Scheffer, C. (2008). Benchmarking of a full-body inertial motion capture system for clinical gait analysis. 2008 *30th Annual International Conference of the IEEE Engineering in Medicine and Biology Society*, 2008, 4579–4582. https://doi.org/10.1109/IEMBS.2008.4650232

Cooper, G., Sheret, I., McMillian, L., Siliverdis, K., Sha, N., Hodgins, D., Kenney, L., & Howard, D. (2009). Inertial sensor-based knee flexion/extension angle estimation. *Journal of Biomechanics*, 42(16), 2678–2685. https://doi.org/10.1016/j.jbiomech.2009.08.004

De Guise, J., Mezghani, N., Aissaoui, R., & Hagemeister, N. (2011). New comprehensive methods for the biomechanical analysis of knee osteoarthritis. In: Pelletier, J. M., Pelletier, J. P., Understanding osteoarthritis from bench to bedside. Kerala, India: *Research Signpost*, 85-102.

Dejnabadi, H., Jolles, B. M., & Aminian, K. (2005). A new approach to accurate measurement of uniaxial joint angles based on a combination of accelerometers and gyroscopes. *IEEE Transactions on Biomedical Engineering*, 52(8), 1478–1484. https://doi.org/10.1109/TBME.2005.851475

Determine Orientation Using Inertial Sensors. (n.d). MathWorks. Retrieved from https://www.mathworks.com/help/fusion/gs/determine-orientation-through-sensor-fusion.html

Favre, J., Jolles, B. M., Aissaoui, R., & Aminian, K. (2008). Ambulatory measurement of 3D knee joint angle. *Journal of Biomechanics*, 41(5), 1029–1035. https://doi.org/10.1016/j.jbiomech.2007.12.003

Gage, J. R. (1990). Surgical treatment of knee dysfunction in cerebral palsy. *Clinical Orthopaedics and Related Research*, 253, 45–54. https://doi.org/10.1097/00003086-199004000-00008

Gupton, M., Imonugo, O., & Terreberry, R. (2022). Anatomy, Bony Pelvis and Lower Limb, Knee. *Statpearls Publishing*. Retrieved from https://www.ncbi.nlm.nih.gov/books/NBK500017/

Iosa, M., Picerno, P., Paolucci, S., & Morone, G. (2016). Wearable inertial sensors for human movement analysis. *Expert Review of Medical Devices*, 13(7), 641–659. https://doi.org/10.1080/17434440.2016.1198694

Jadhav, S. P., More, S. R., Riascos, R. F., Lemos, D. F., & Swischuk, L. E. (2014). Comprehensive review of the anatomy, function, and imaging of the popliteus and associated pathologic conditions. *Radiographics*, 34(2), 496–513. https://doi.org/10.1148/rg.342125082

Kayaalp, M., Agres, A., Reichmann, J., Bashkuev, M., Duda, G., & Becker, R. (2019). Validation of a Novel Device for the Knee Monitoring of Orthopaedic Patients. *Sensors*, 19(23), 5193. doi: 10.3390/s19235193

Kim, H., Kim, K., Yang, D., Jeung, S., Choi, H., & Choy, W. (2015). Screw-Home Movement of the Tibiofemoral Joint during Normal Gait: Three-Dimensional Analysis. *Clinics In Orthopedic Surgery*, 7(3), 303. doi: 10.4055/cios.2015.7.3.303

Kiriella, J. B., Di Bacco, V. E., Hollands, K. L., & Gage, W. H. (2020). Evaluation of the Effects of Prescribing Gait Complexity Using Several Fluctuating Timing Imperatives. *Journal of Motor Behavior*, 52(5), 570–577. https://doi.org/10.1080/00222895.2019.1654971

Marker Set Guidelines. (2017, August 15). C-Motion Wiki Documentation. Retrieved January 18, 2024, from https://cmotion.com/v3dwiki/index.php?title=Marker_Set_Guidelines#Coda_Pelvis_and_Helen_Hayes_Pelvis

Marmelat, V., Torre, K., Beek, P., & Daffertshofer, A. (2014). Persistent Fluctuations in Stride Intervals under Fractal Auditory Stimulation. *Plos ONE*, 9(3), e91949. doi: 10.1371/journal.pone.0091949

Nazarahari, M., & Rouhani, H. (2021). 40 years of sensor fusion for orientation tracking via magnetic and inertial measurement units: Methods, lessons learned, and future challenges. *Information Fusion*, 68, 67–84. https://doi.org/10.1016/j.inffus.2020.10.018

NXP. (2015). *Freescale Sensor Fusion Library for Kinetis MCUs*. Freescale Semiconductor, Inc. https://www.nxp.com/docs/en/data-sheet/XSFLK_DS.pdf

Park, S., & Yoon, S. (2021). Validity Evaluation of an Inertial Measurement Unit (IMU) in Gait Analysis Using Statistical Parametric Mapping (SPM). *Sensors*, 21(11), 3667. doi: 10.3390/s21113667

Robert-Lachaine, X., Mecheri, H., Larue, C., & Plamondon, A. (2016). Validation of inertial measurement units with an optoelectronic system for whole-body motion analysis. *Medical & Biological Engineering & Computing*, 55(4), 609-619. doi: 10.1007/s11517-016-1537-2

Robertson, D. G., Caldwell, G. E., Hamill, J., Kamen, G., & Whittlesey, S. N. (2014). *Research methods in biomechanics* (Second edition.). Human Kinetics.

Sasiadek, J. Z. (2002). Sensor Fusion. *Annual Reviews in Control*, 26(2), 203-228. https://doi.org/10.1016/S1367-5788(02)00045-7

Seel, T., Raisch, J., & Schauer, T. (2014). IMU-Based Joint Angle Measurement for Gait Analysis. *Sensors*, 14(4), 6891-6909. doi: 10.3390/s140406891

Tian, S., Yang, W., Grange, J. M. L., Wang, P., Huang, W., & Ye, Z. (2019). Smart healthcare: making medical care more intelligent. *Global Health Journal*, 3(3), 62–65. https://doi.org/10.1016/j.glohj.2019.07.001

Takeda, R., Tadano, S., Natorigawa, A., Todoh, M., & Yoshinari, S. (2009). Gait posture estimation using wearable acceleration and gyro sensors. *Journal of Biomechanics*, 42(15), 2486–2494. https://doi.org/10.1016/j.jbiomech.2009.07.016

Widodo, R. B., & Wada, C. (2016). Attitude Estimation Using Kalman Filtering: External Acceleration Compensation Considerations. *Journal of Sensors*, 2016, 1–24. https://doi.org/10.1155/2016/6943040

Winter, D. A. (2009). *Biomechanics and Motor Control of Human Movement* (4th ed.). John Wiley & Sons, Inc.

Zügner, R., Tranberg, R., Timperley, J., Hodgins, D., Mohaddes, M., & Kärrholm, J. (2019). Validation of inertial measurement units with optical tracking system in patients operated with Total hip arthroplasty. *BMC Musculoskeletal Disorders*, 20(1), 52–52. https://doi.org/10.1186/s12891-019-2416-4